National Centre for Earth Observation
NATURAL ENVIRONMENT RESEARCH COUNCIL

UNIVERSITY OF LEICESTER

esa

→ 8th ADVANCED TRAINING COURSE ON LAND REMOTE SENSING

10–14 September 2018
University of Leicester | United Kingdom

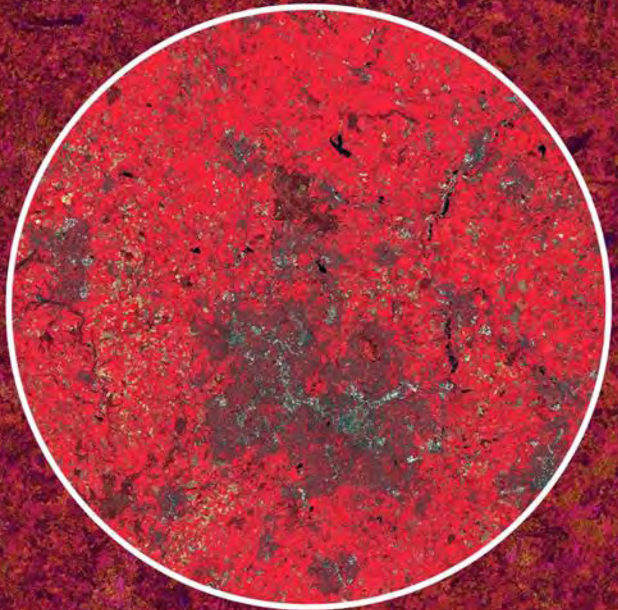

Urban Mapping

Sebastian van der Linden, Akpona Okujeni, Franz Schug

11/09/2018

Introduction to urban remote sensing

Introduction – The urban millennium

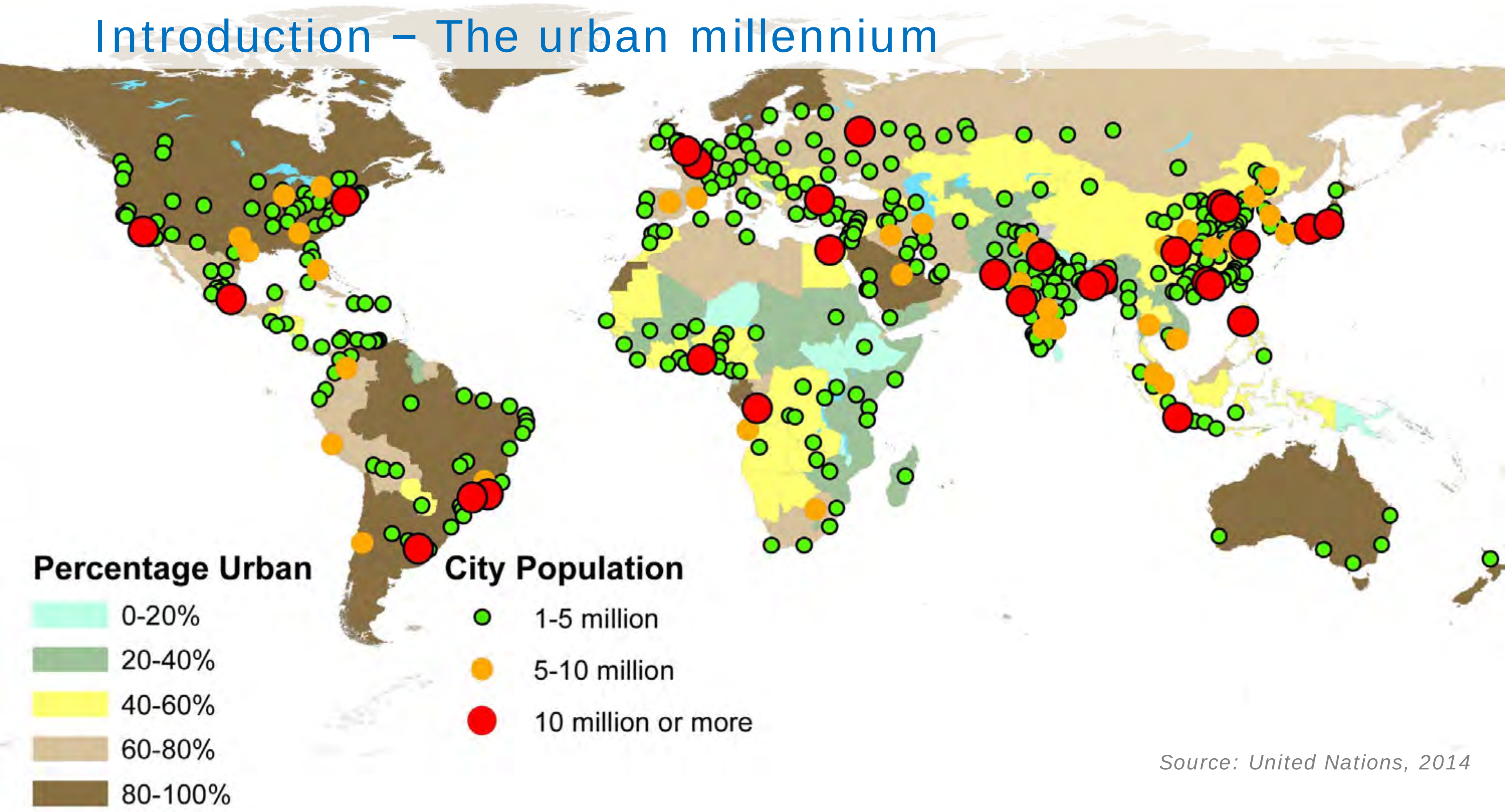

Source: United Nations, 2014

Urban areas mark extremes in terms of human domestication of nature.

Urban environments are very diverse in terms of size, shape, material composition and fragmentation.

Source: Google Earth

Urban areas from space

30x30 km footprint of Berlin, Germany, as seen by

UL: Landsat 8 (swIR, nIR, red)

UR: Landsat 8 thermal

LL: Sentinel-1A

LR: vis. nightlights (ISS photo).

Each sensor system provides complementary information, but is also subject to non-uniqueness.

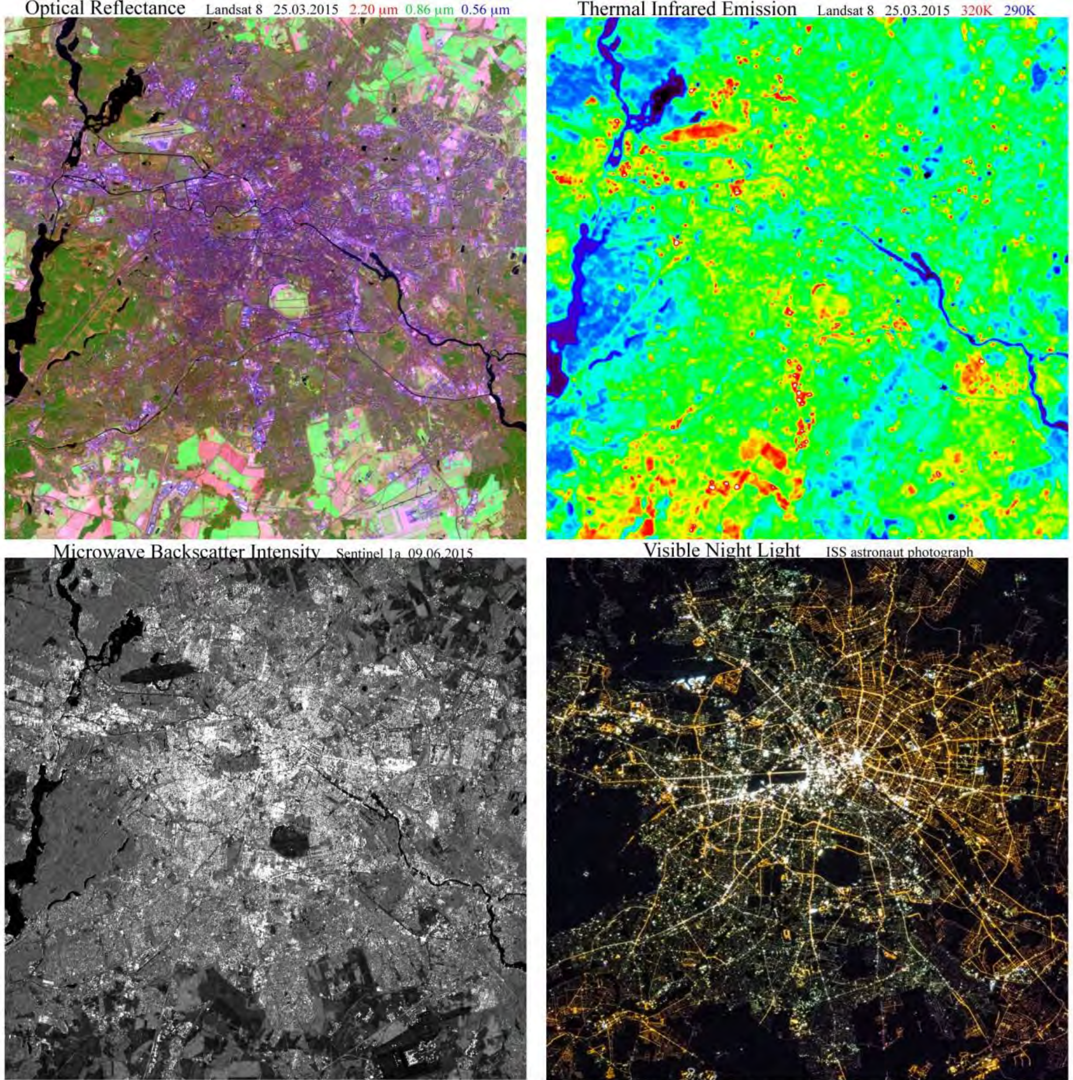

Source: Small et al., 2018

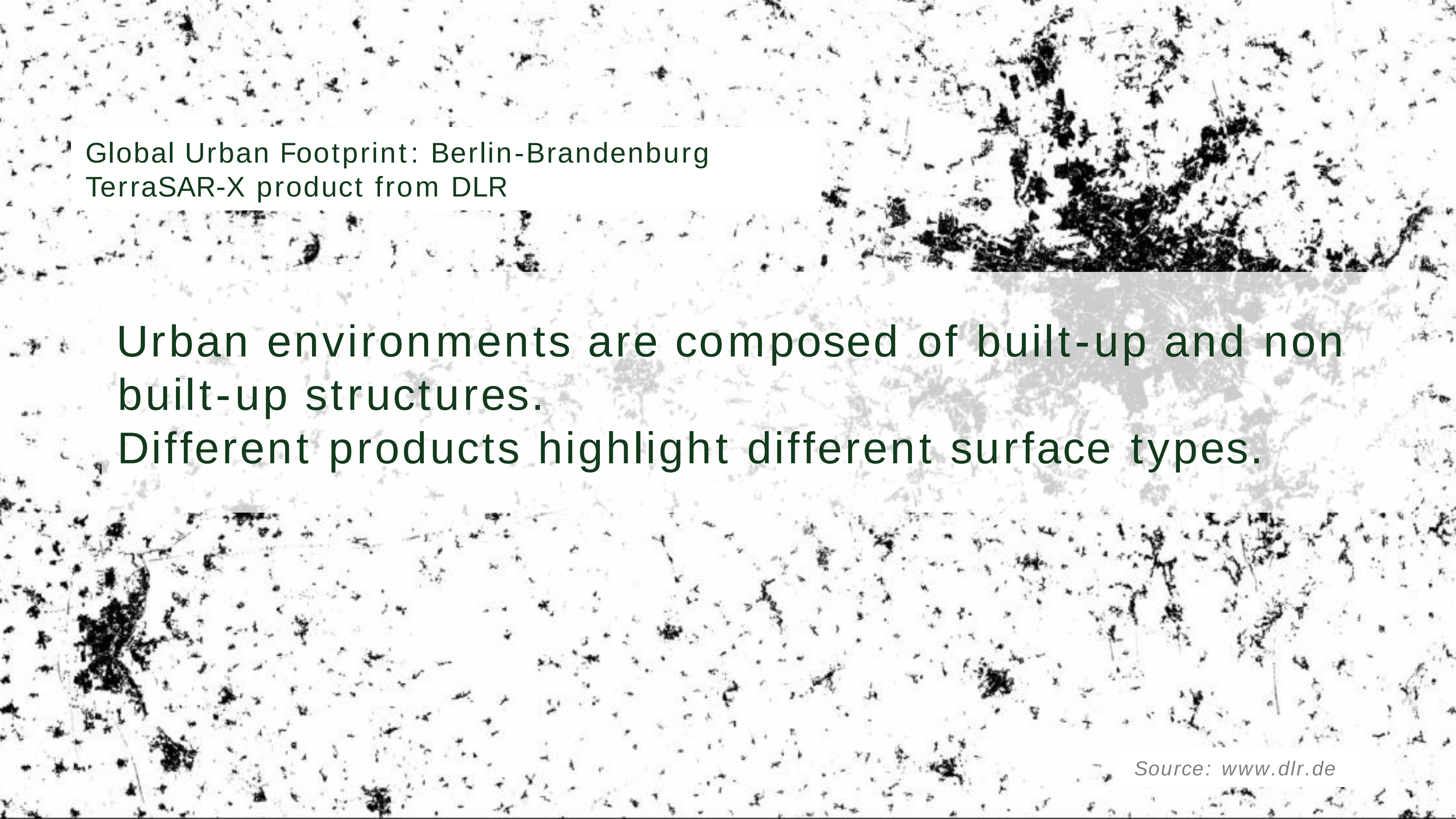

Global Urban Footprint: Berlin-Brandenburg
TerraSAR-X product from DLR

Urban environments are composed of built-up and non built-up structures.
Different products highlight different surface types.

Source: www.dlr.de

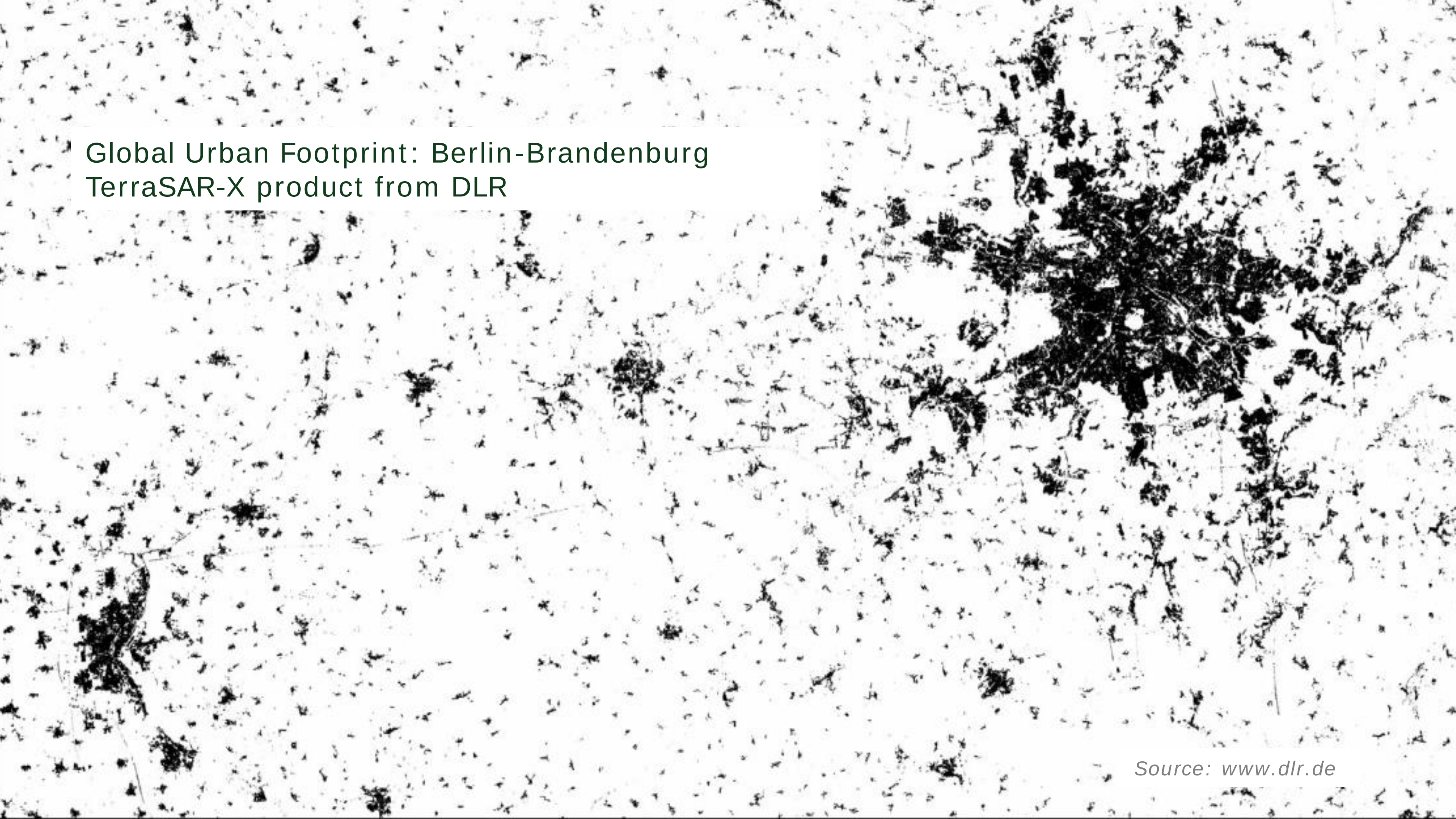
Global Urban Footprint: Berlin-Brandenburg
TerraSAR-X product from DLR
Source: www.dlr.de

Global Human Settlement layer: Berlin-Brandenburg
Multi-sensor product from JRC

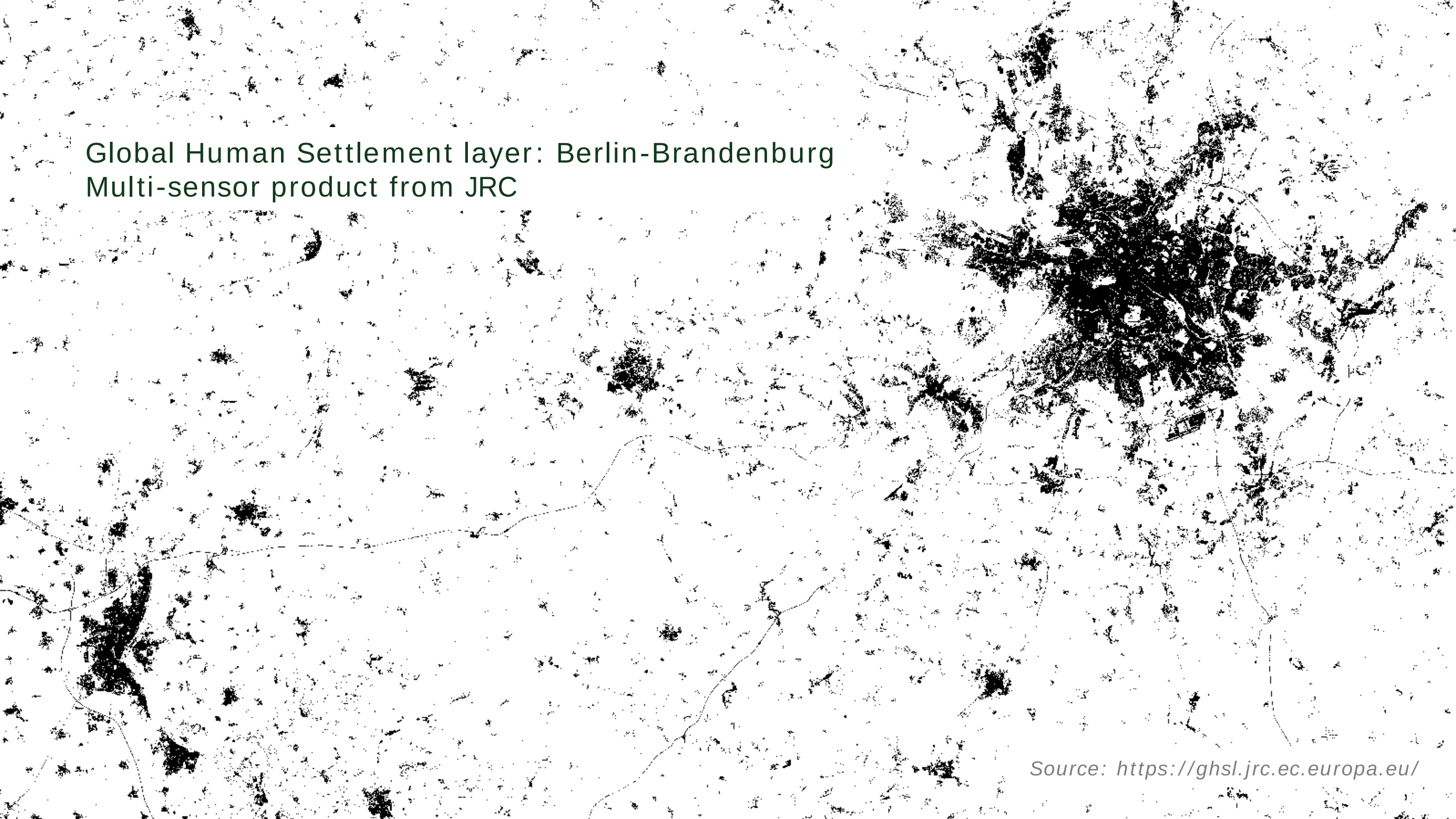

Source: https://ghsl.jrc.ec.europa.eu/

European Urban Atlas: Berlin-Brandenburg
Multi-sensor product of EEA

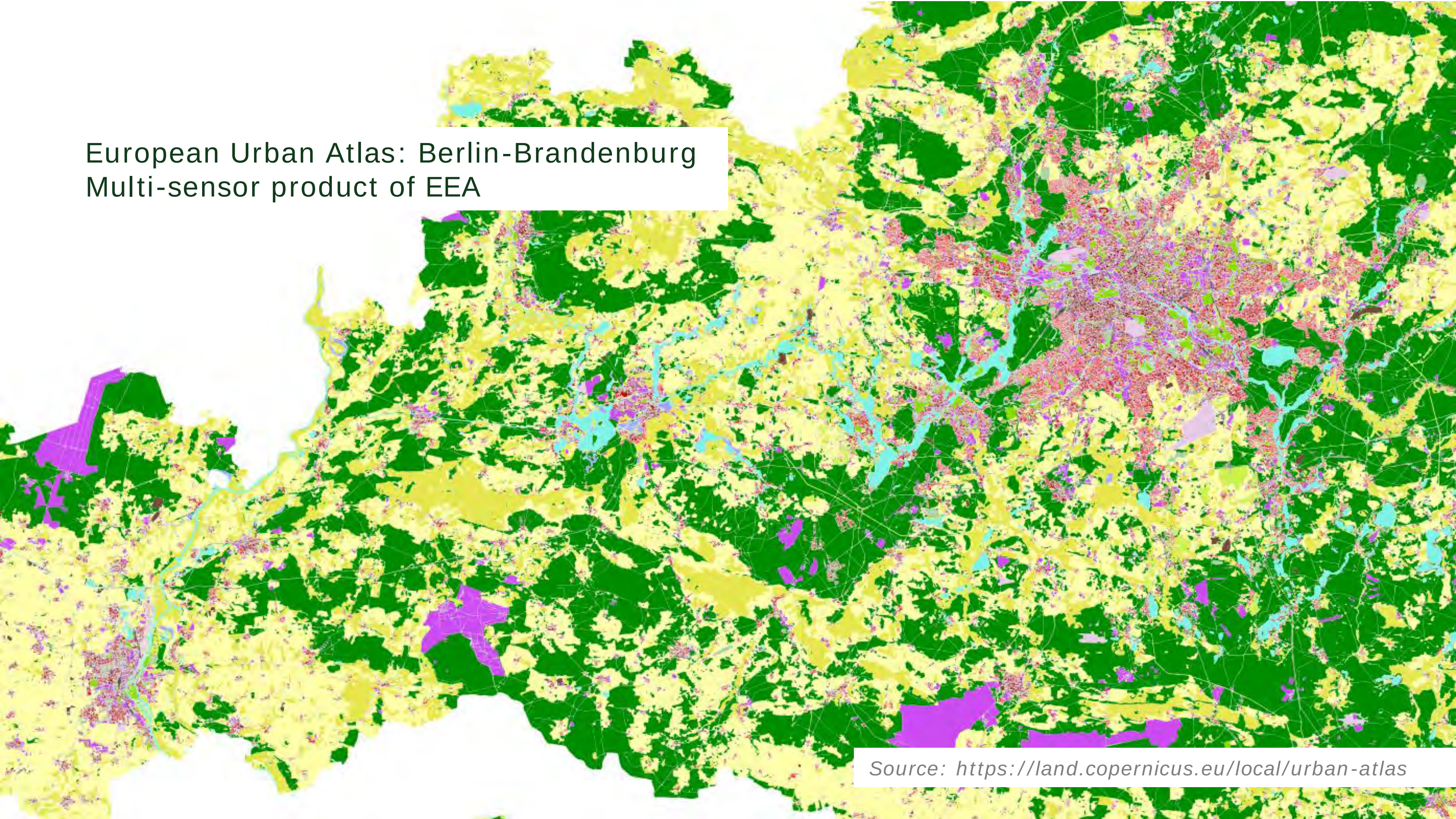

Source: https://land.copernicus.eu/local/urban-atlas

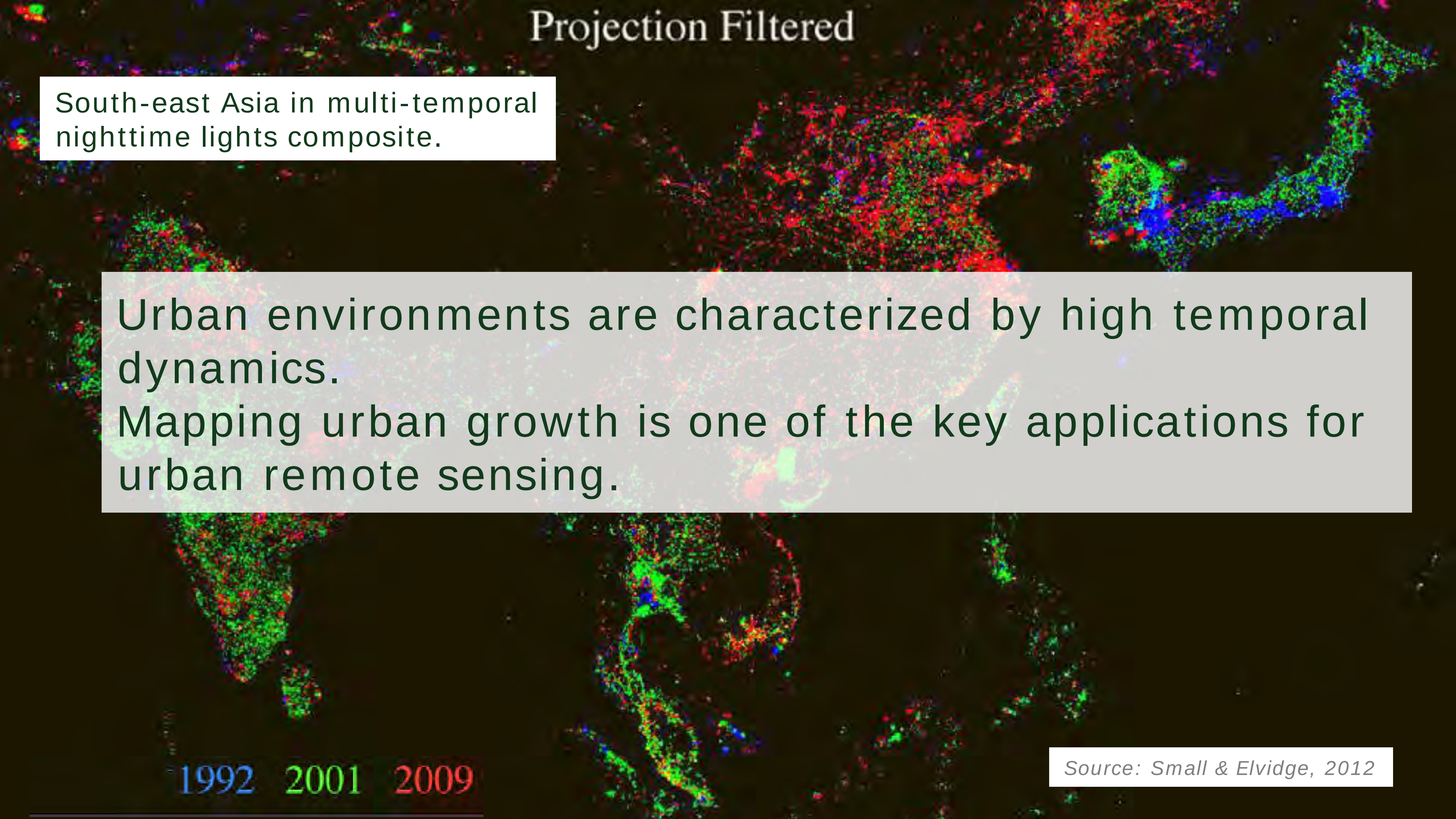

South-east Asia in multi-temporal nighttime lights composite.

Urban environments are characterized by high temporal dynamics.
Mapping urban growth is one of the key applications for urban remote sensing.

Source: Small & Elvidge, 2012

A detailed description of urban composition (ideally at sub-pixel level) is needed for environmental analysis. Remote sensing contributes to urban planning, micro climatology, hydrology, hazard or habitat modelling, etc.

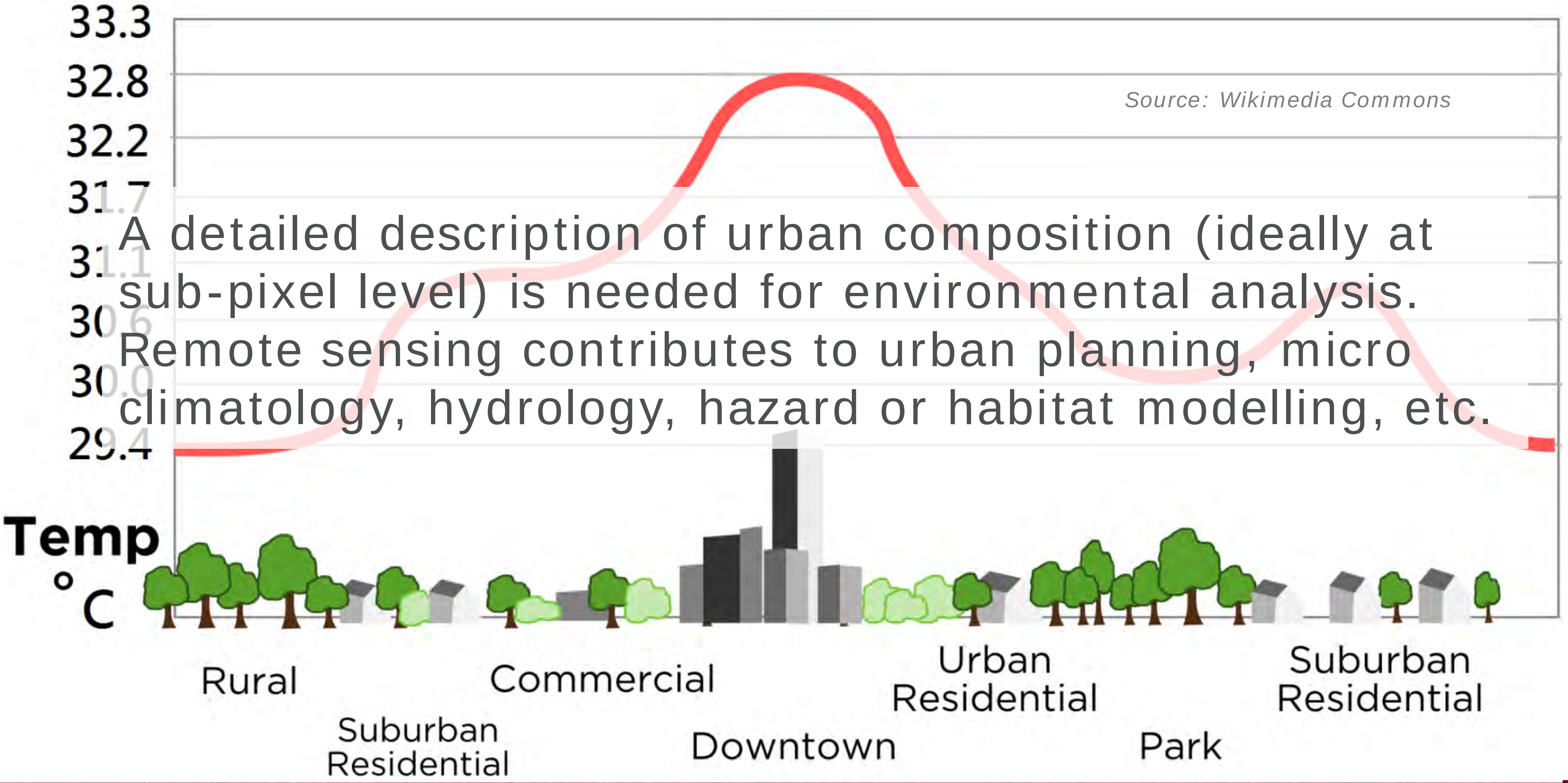

Introduction (summary)

With more than have of the world's population living in cities and rapid urbanization rates, remote sensing plays a pivotal role in monitoring urban environments.

Especially in less developed countries and for fast growing urban agglomerations remote sensing is often the only reliable source of spatial information.

Most urban environmental models use remote sensing based maps as input.

Remote sensing analyses usually focus on

- mapping urban extent and growth
- mapping urban composition

Characteristics and challenges of urban remote sensing

Urban land cover

Urban land cover is characterized by great diversity of materials. Here the city of Berlin, Germany.

Source: Google Earth

Urban land cover

Urban land cover classes can be hierarchically organized down to the material level.

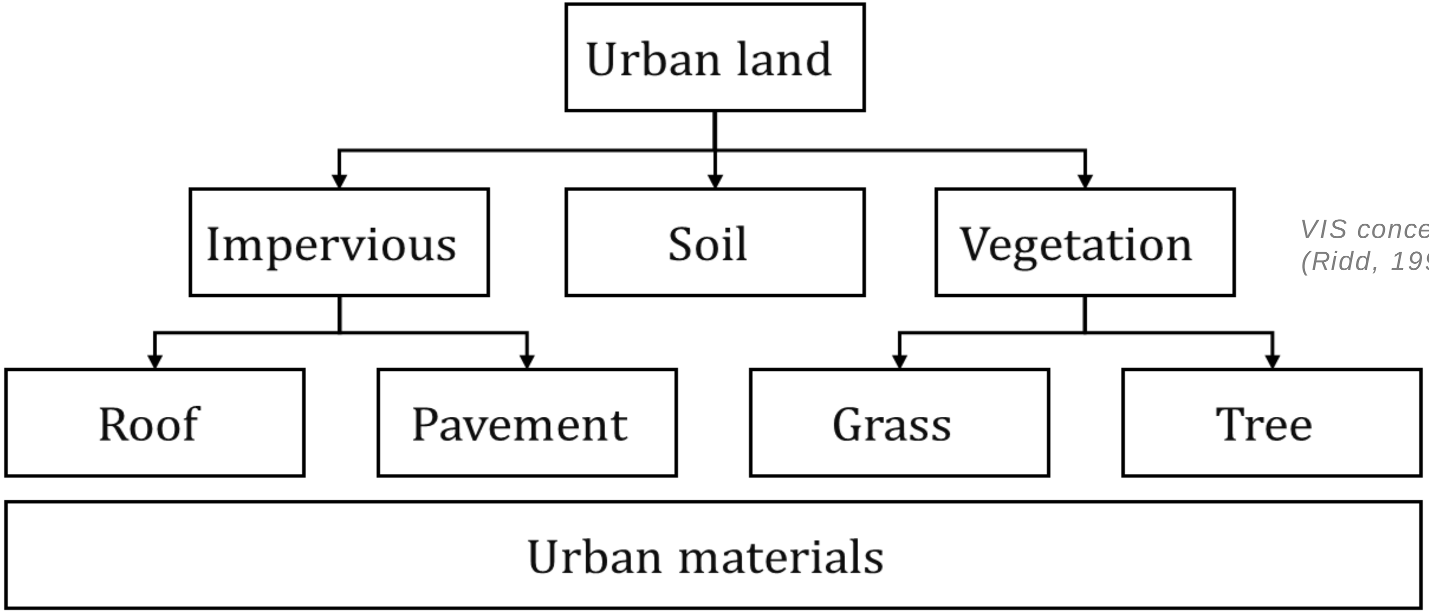

VIS concept (Ridd, 1995)

Urban land cover

High *spectral* diversity of construction materials and natural surface types.

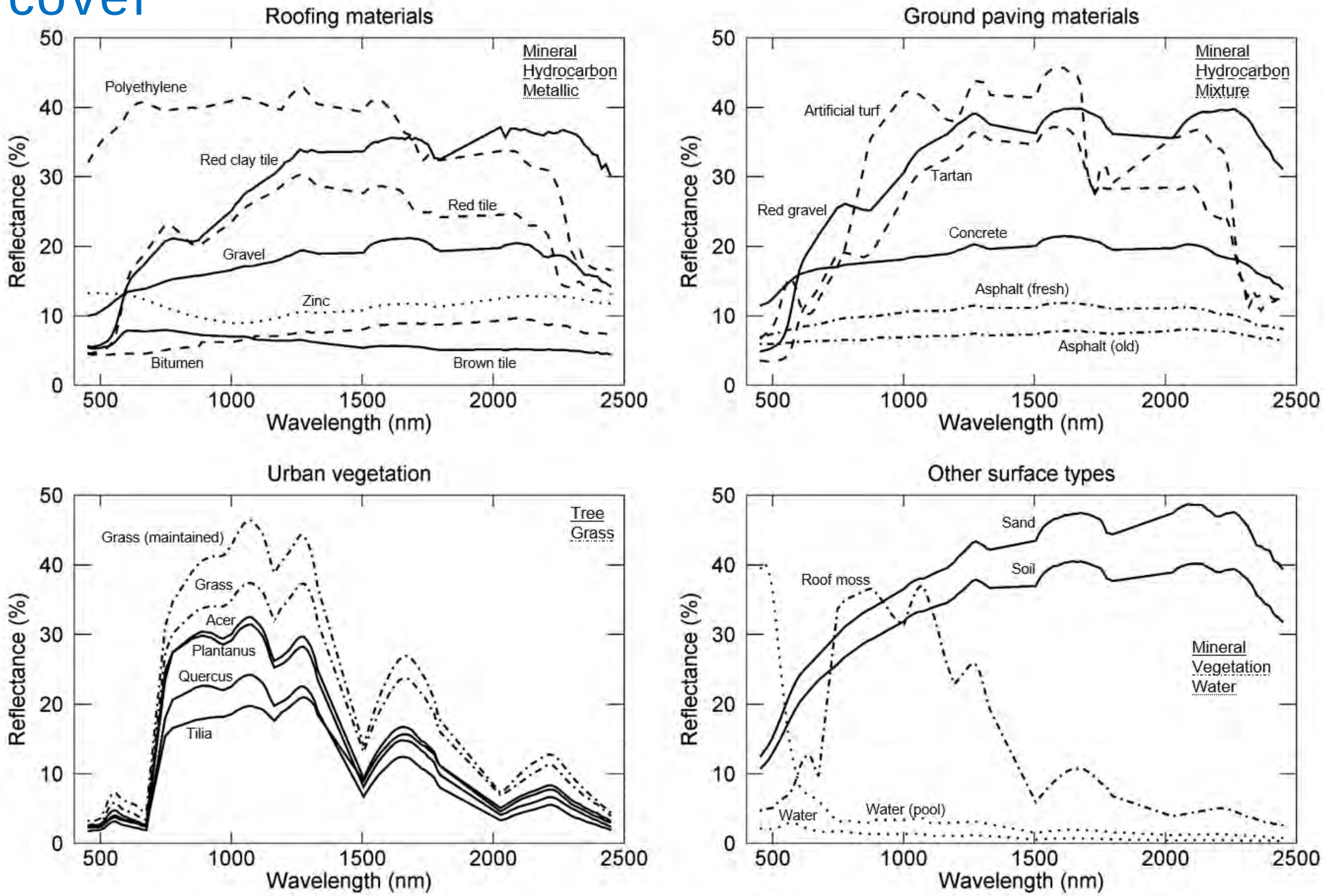

Source: Small et al., 2018

Urban land cover

Polarimetric *SAR* representation of Berlin area and three subsets using TerraSAR-X StripMap data in the Pauli color coding scheme (R: HH-VV, G: HV, B: HH+VV).

Mirror-like reflectors appear dark (streets, sport fields, water). Vegetation is dark greenish with HV dominating. Strong backscatter structure appear bright, with the actual color (green to pink) also depending on object size, geometric arrangement and orientation.

Source: Small et al., 2018

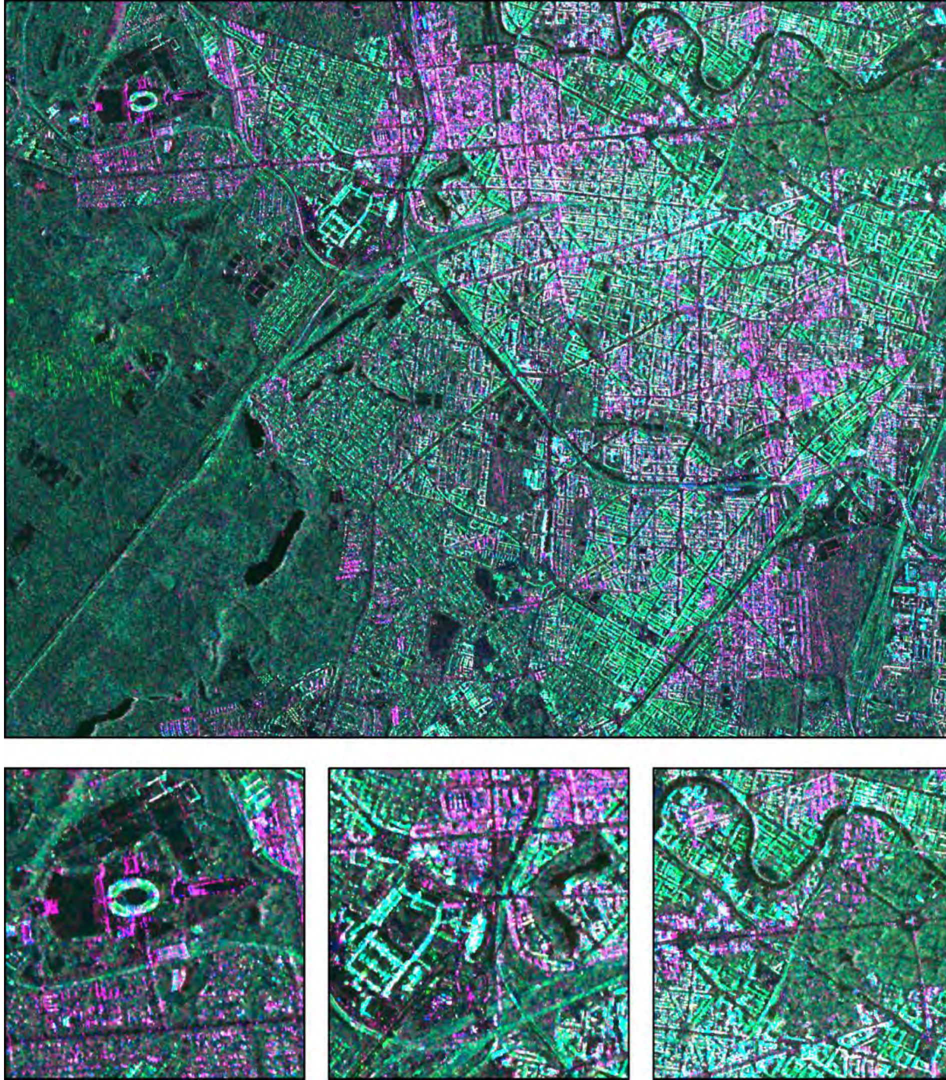

Urban land cover

Berlin area *thermal* emissions in July and September during day (top, Landsat-7) and night (bottom, Landsat-8).

Water bodies show low values at day and highest at night. Urban forests are always in mid-ranges. Street canyons and large buildings store energy longer and emit even at nighttime.

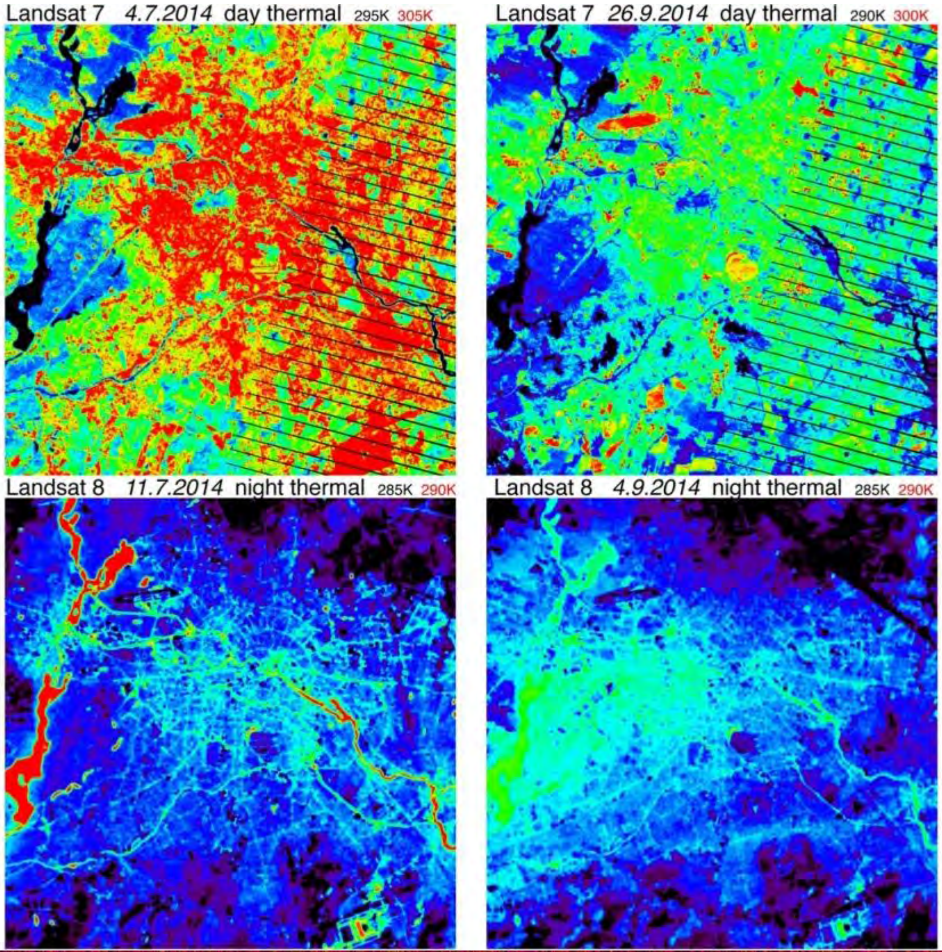

Source: Small et al., 2018

The factor scale in urban remote sensing

Step from approx. <1 m to 30 m leads to massive spatial aggregation.

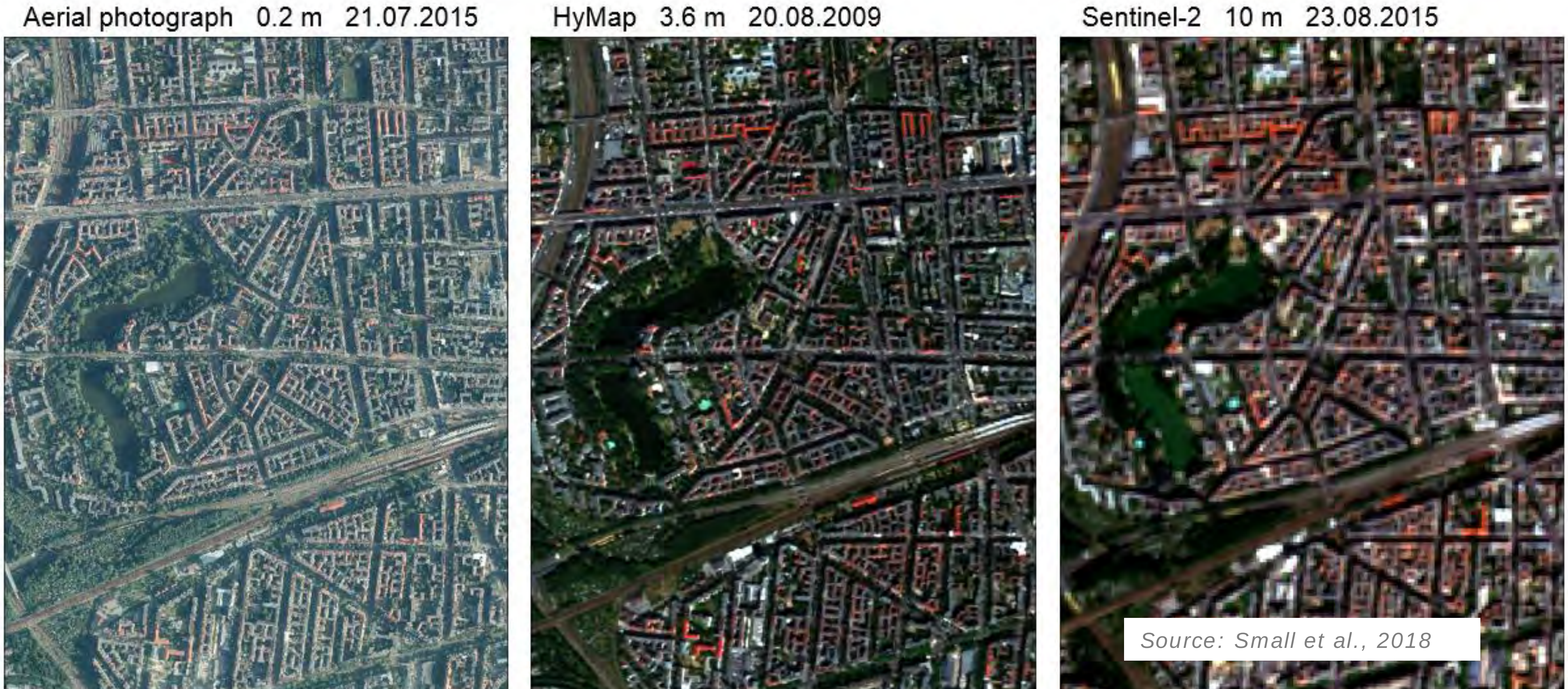

Source: Small et al., 2018

The factor scale in urban remote sensing

Step from approx. 5 m to 30 m leads to massive spectral aggregation.

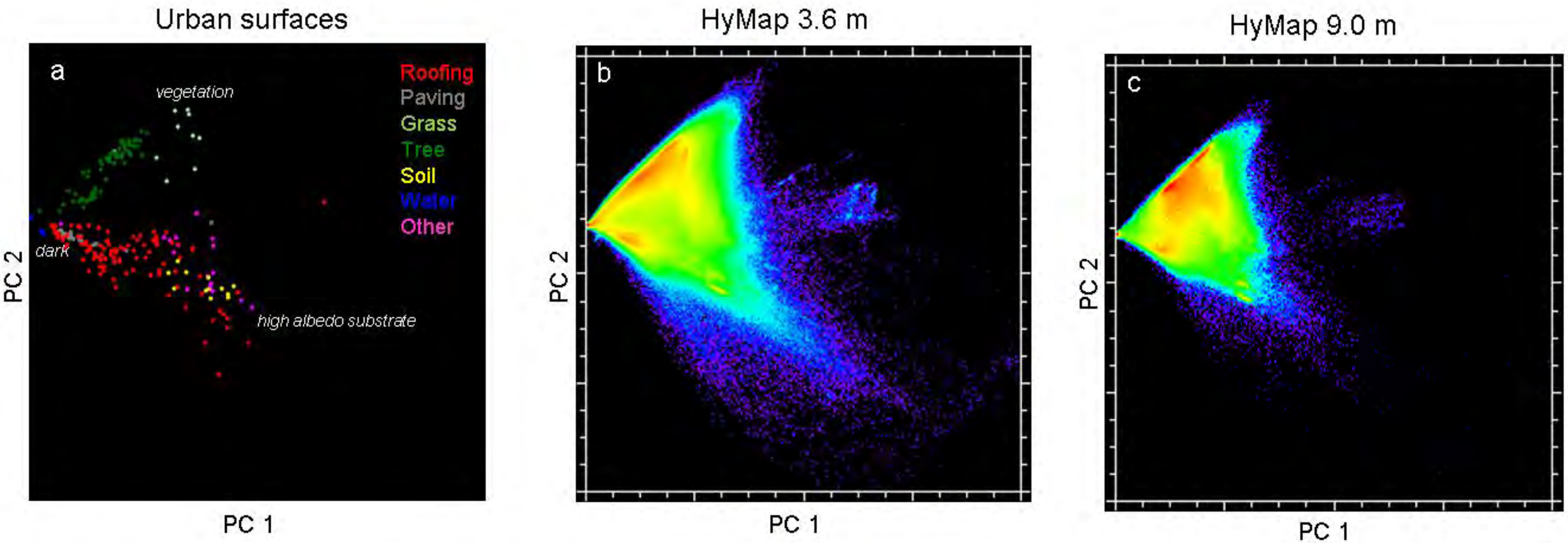

Source: Small et al., 2018

The factor scale in urban remote sensing

High number of mixed pixels.

Complex 3-D geometry and illumination.

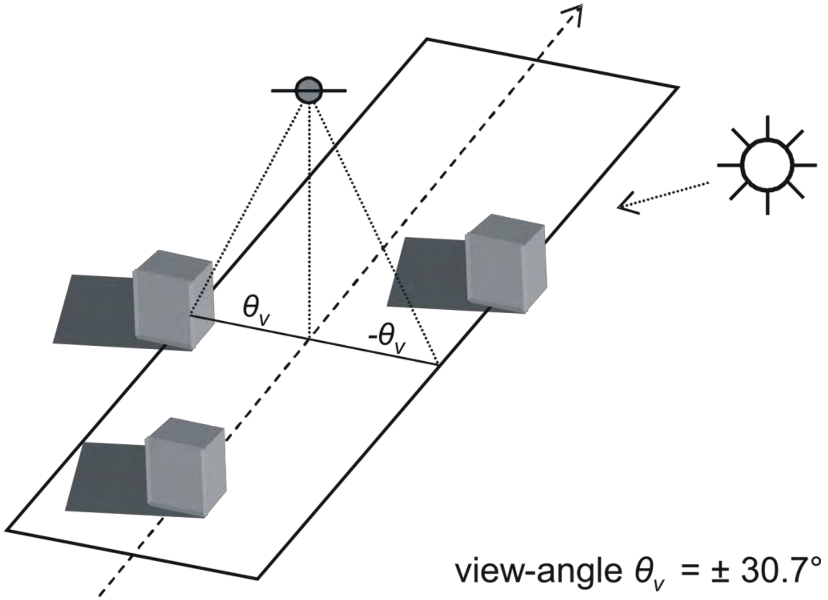

Mapping urban growth and urban composition

Mapping urban growth from optical and SAR data

Urban growth can be mapped reliably by means of remote sensing.

Taubenböck et al. (2012) use data from TerraSAR-X and Landsat to quantify urban growth for global mega cities since 1975 in four time steps.

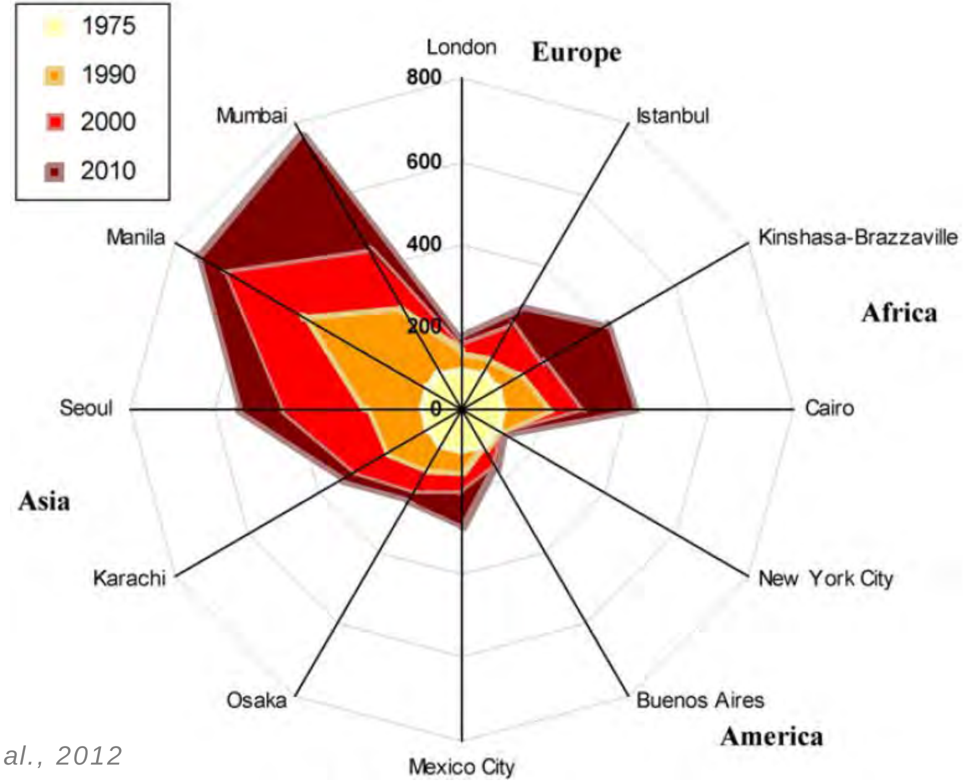

Source: Taubenböck et al., 2012

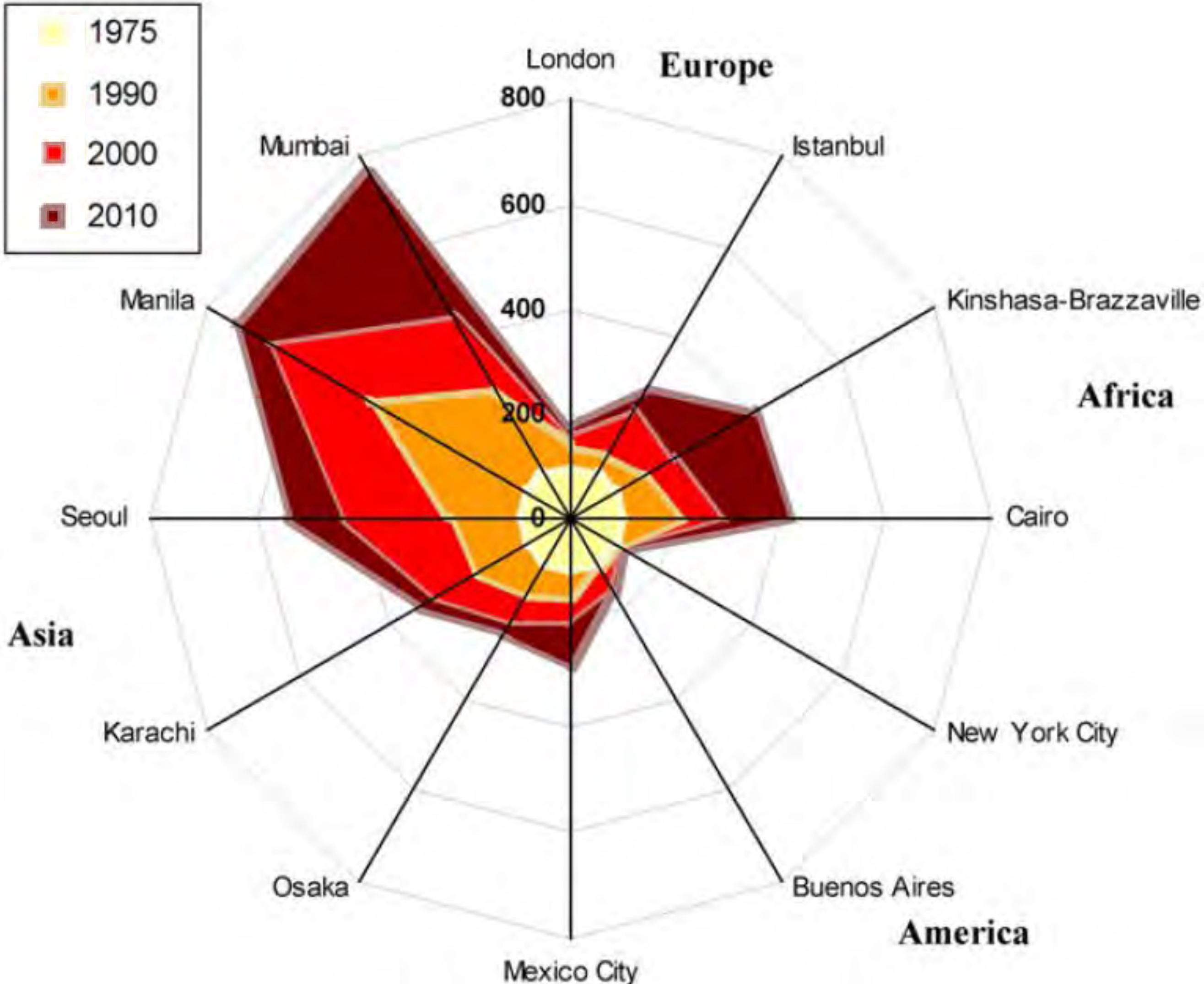

Mega cities are mapped in
1975 – Landsat MSS
1990 – Landsat TM
2000 – Landsat ETM+
2010 – TerraSAR-X

Source: Taubenböck et al., 2012

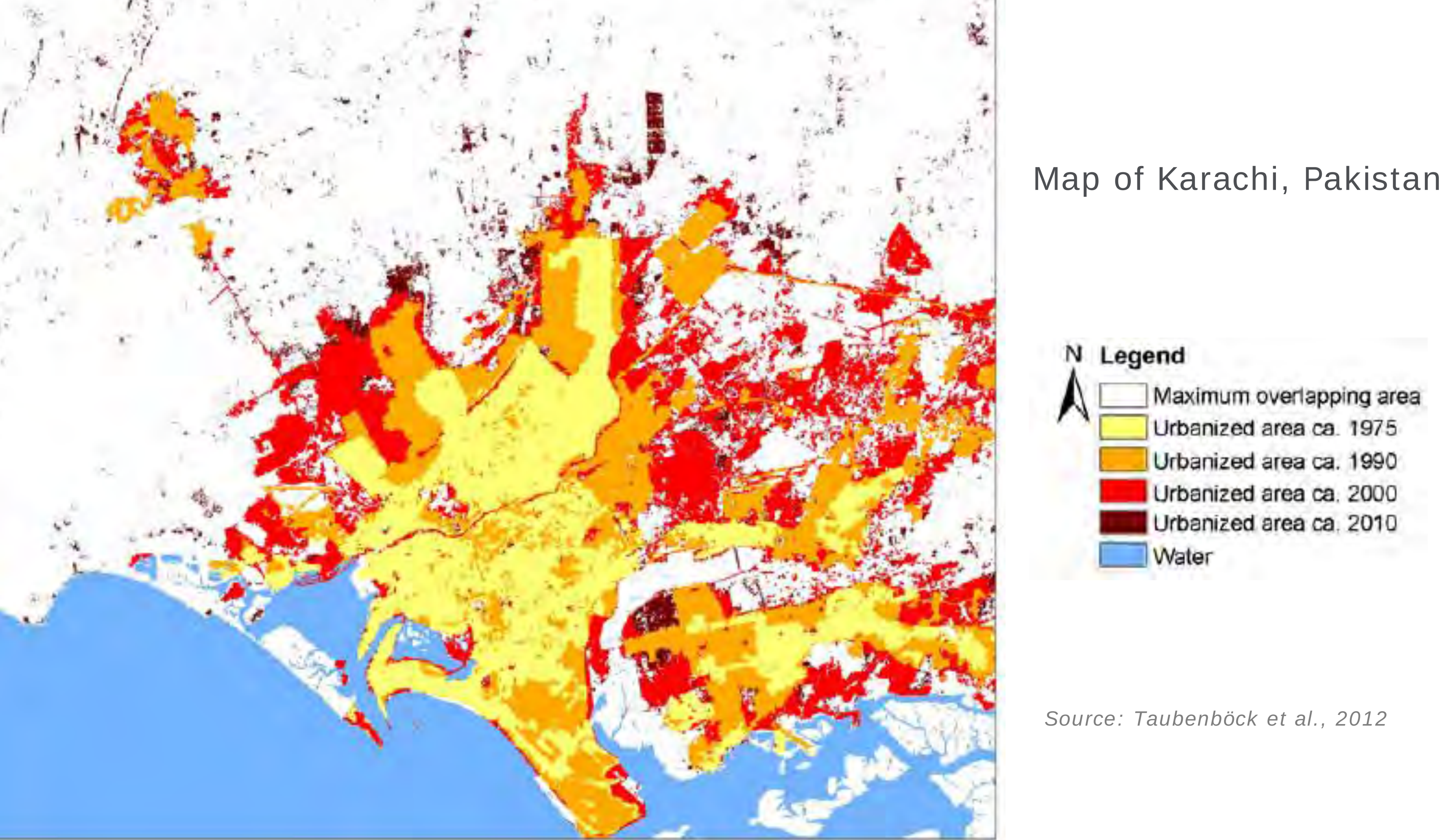

Map of Karachi, Pakistan

Source: Taubenböck et al., 2012

Mapping urban growth from optical data

Urban growth best described by sub-pixel fraction information, e.g. percent built-up cover.

Spectral unmixing or regression analyses needed.

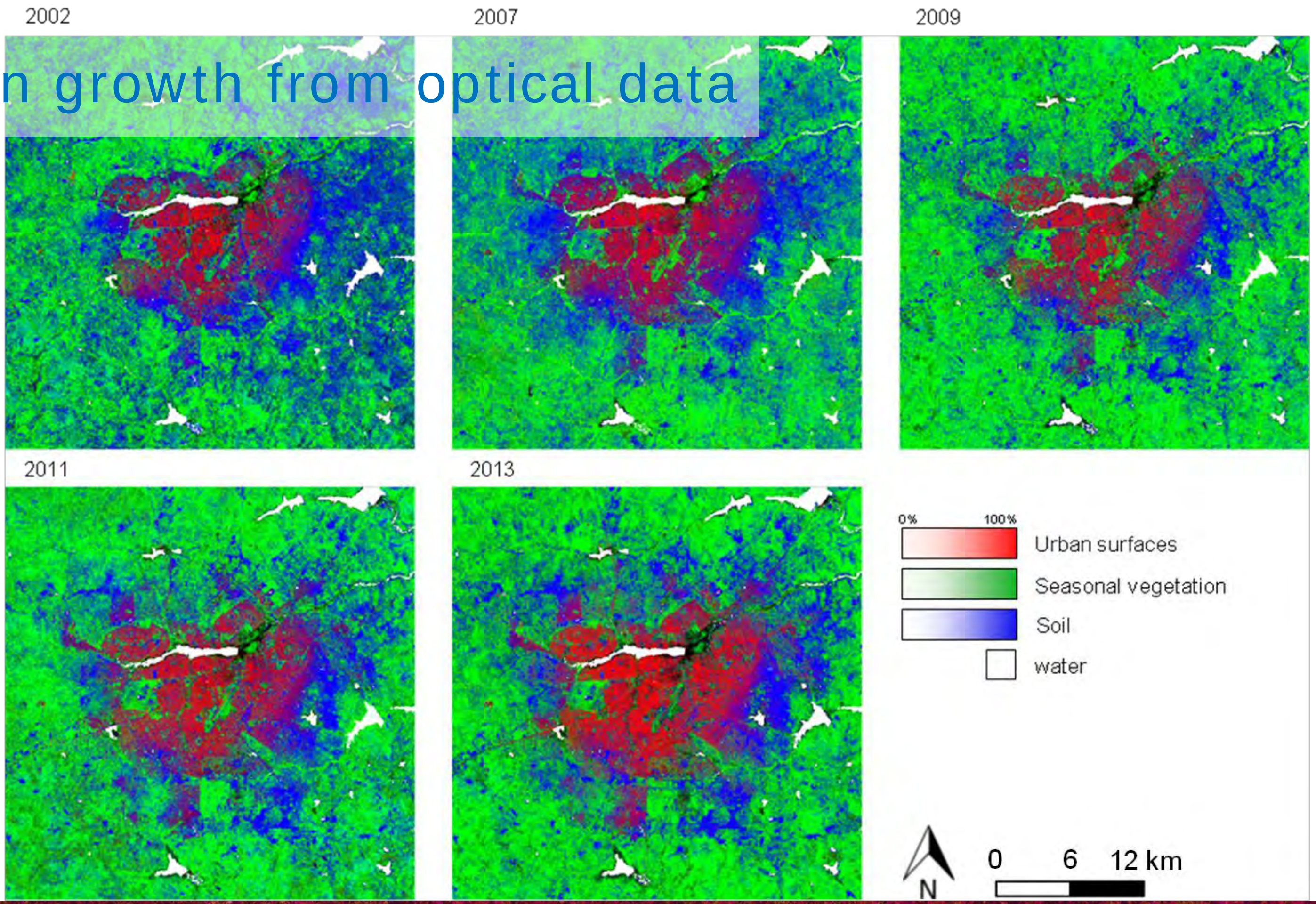

Source: *Schug et al., 2018*

Mapping urban growth from optical data

Information from two seasons allows reliable separation of soil and seasonal vegetation.

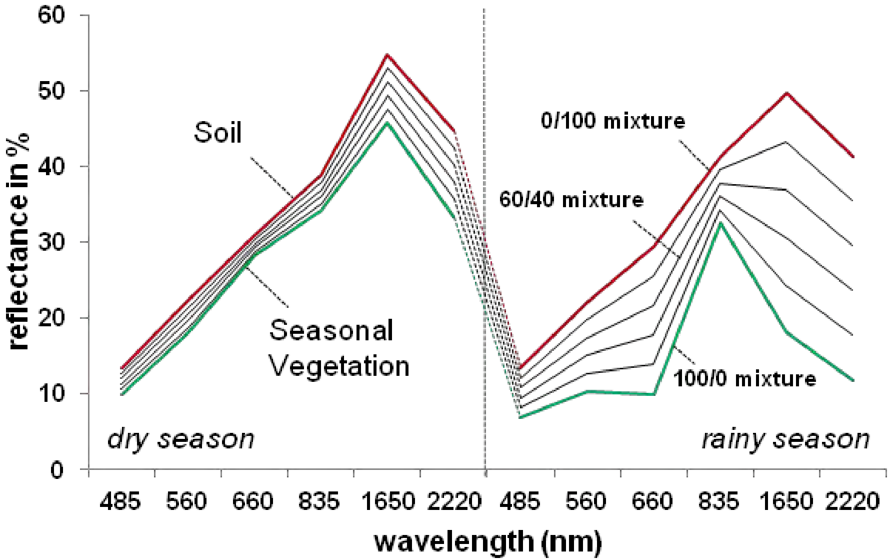

Source: Schug et al., 2018

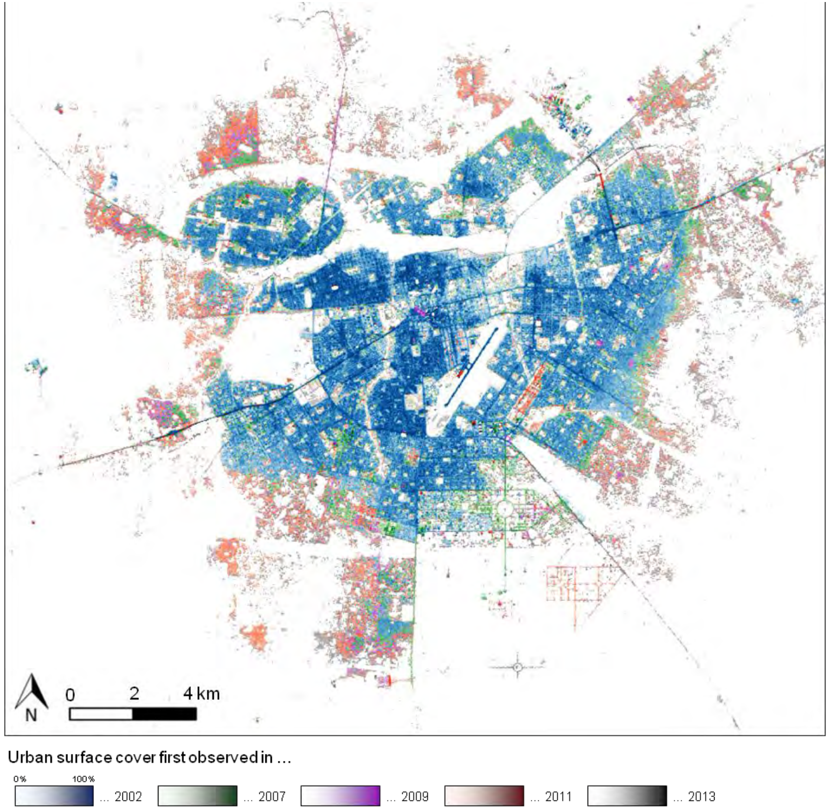

Mapping urban growth from optical data

Sub-pixel fraction allow the description of densification over time better than discrete classification results.

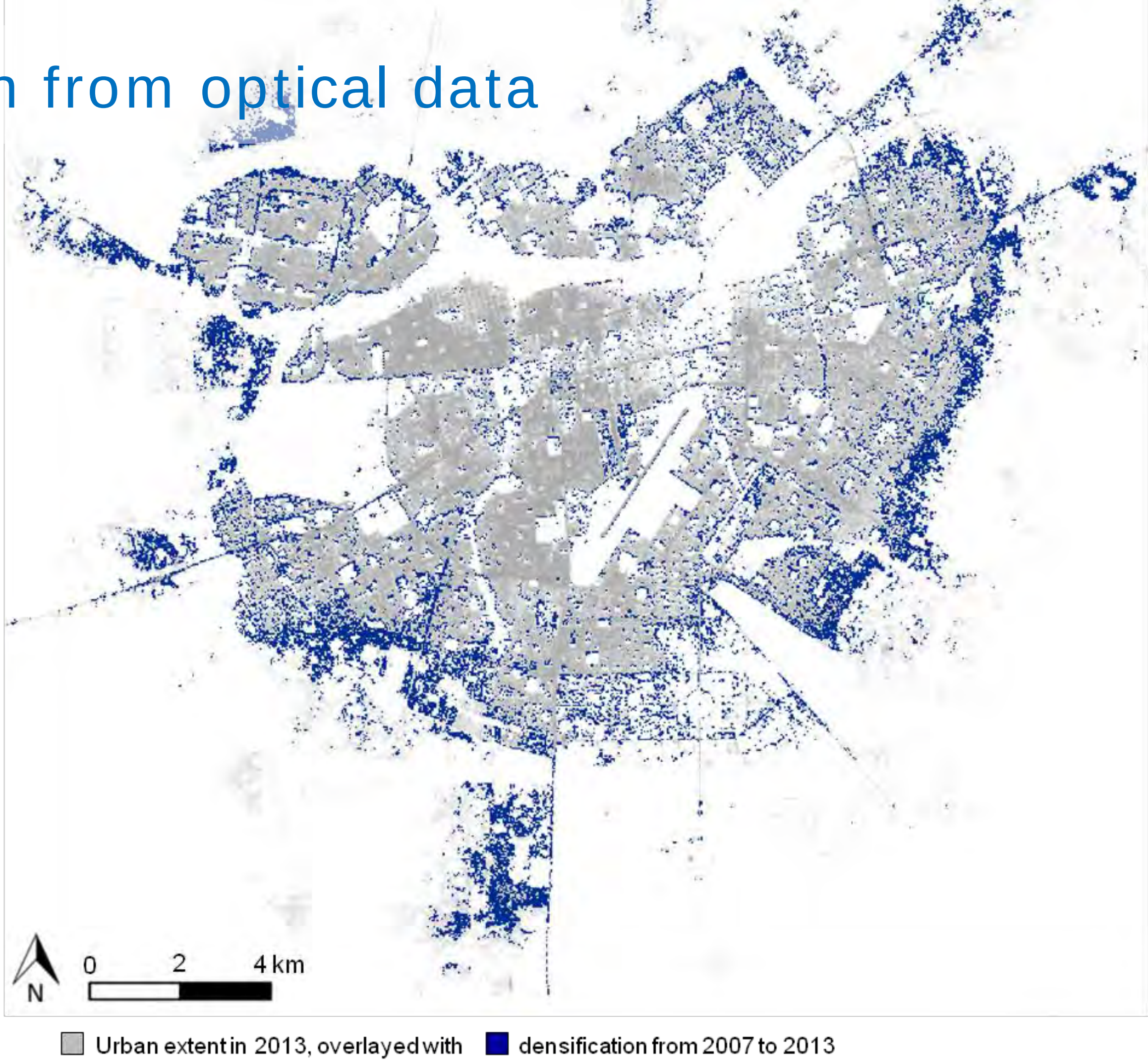

Source: Schug et al., 2018

Mapping urban composition from optical data

Ridd (1995) assumes, every urban pixel is composed of impervious surface, vegetation or soil.
Ridd’s V-I-S concept is based on a thematical framework. It is not based on the spectral characteristics of urban areas.

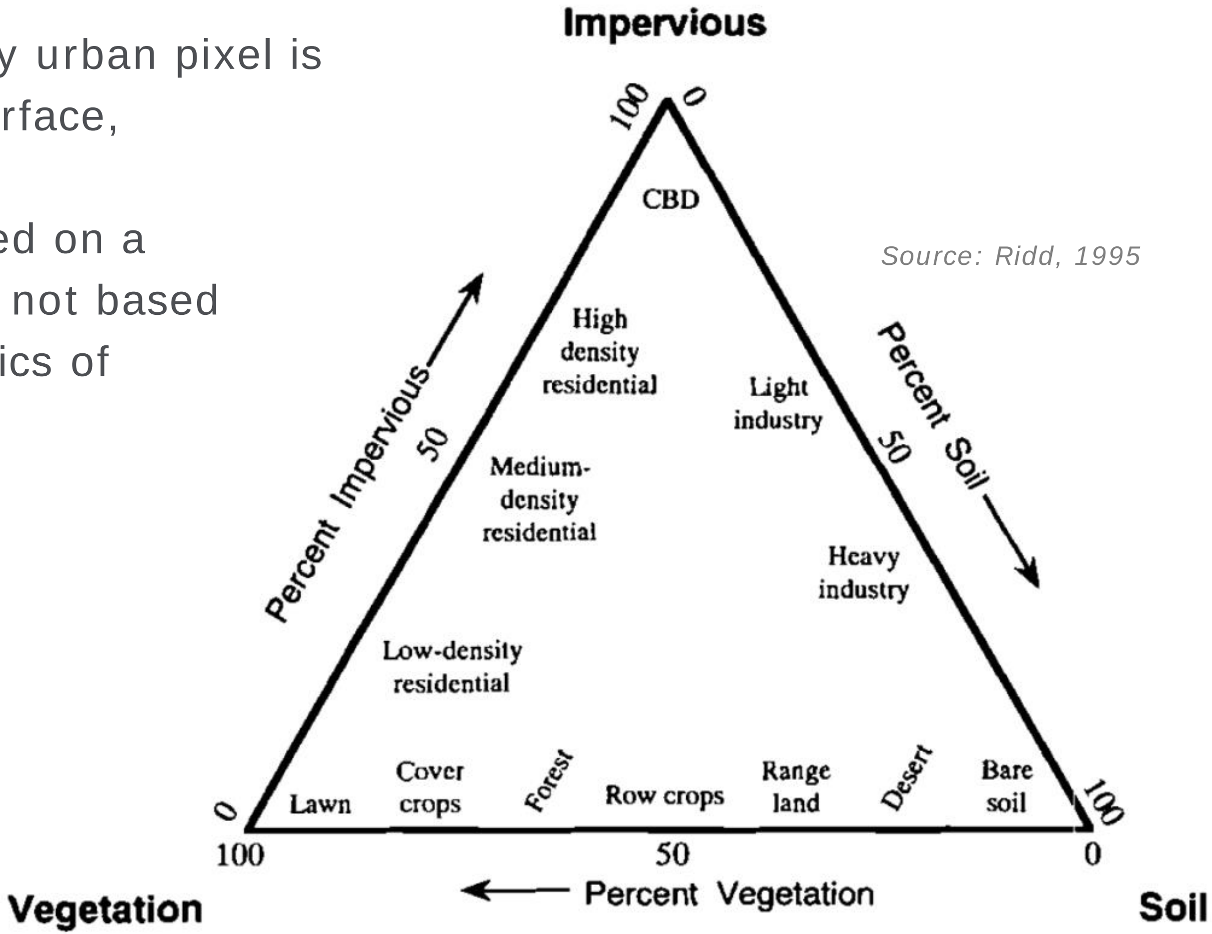

Source: Ridd, 1995

Mapping urban composition from optical data

Small (2005) analysed more than 24 urban areas and concludes that the spectral properties working with Landsat ETM+ always relate to the degree of brightness and the portion of vegetation. This results in a mixing triangle in the first two PC components.

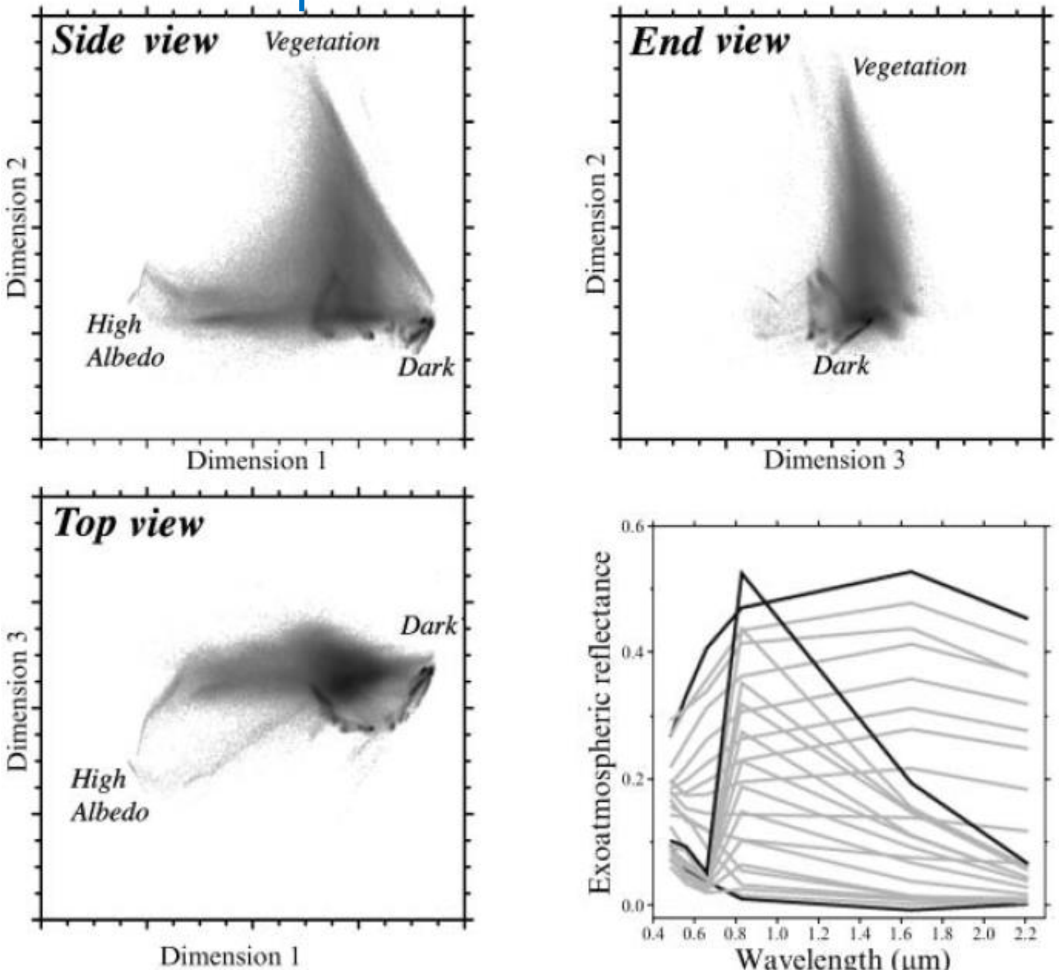

Source: Small, 2005

Mapping urban composition from optical data

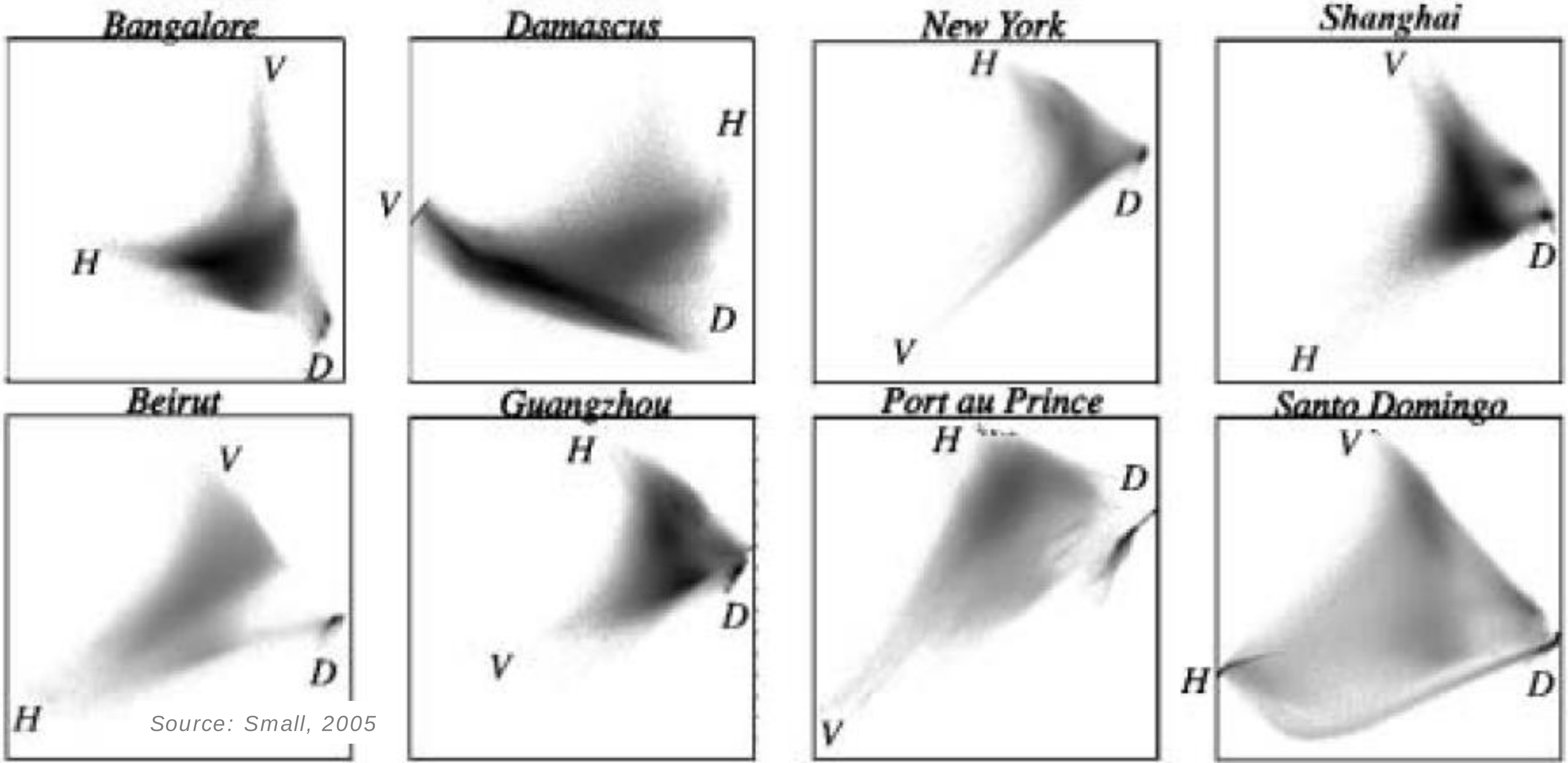

Source: Small, 2005

Mapping urban composition from optical data

Using higher spatial and spectral characteristics with machine learning more urban cover types can be mapped, as e.g. van der Linden et al. (2007) showed.

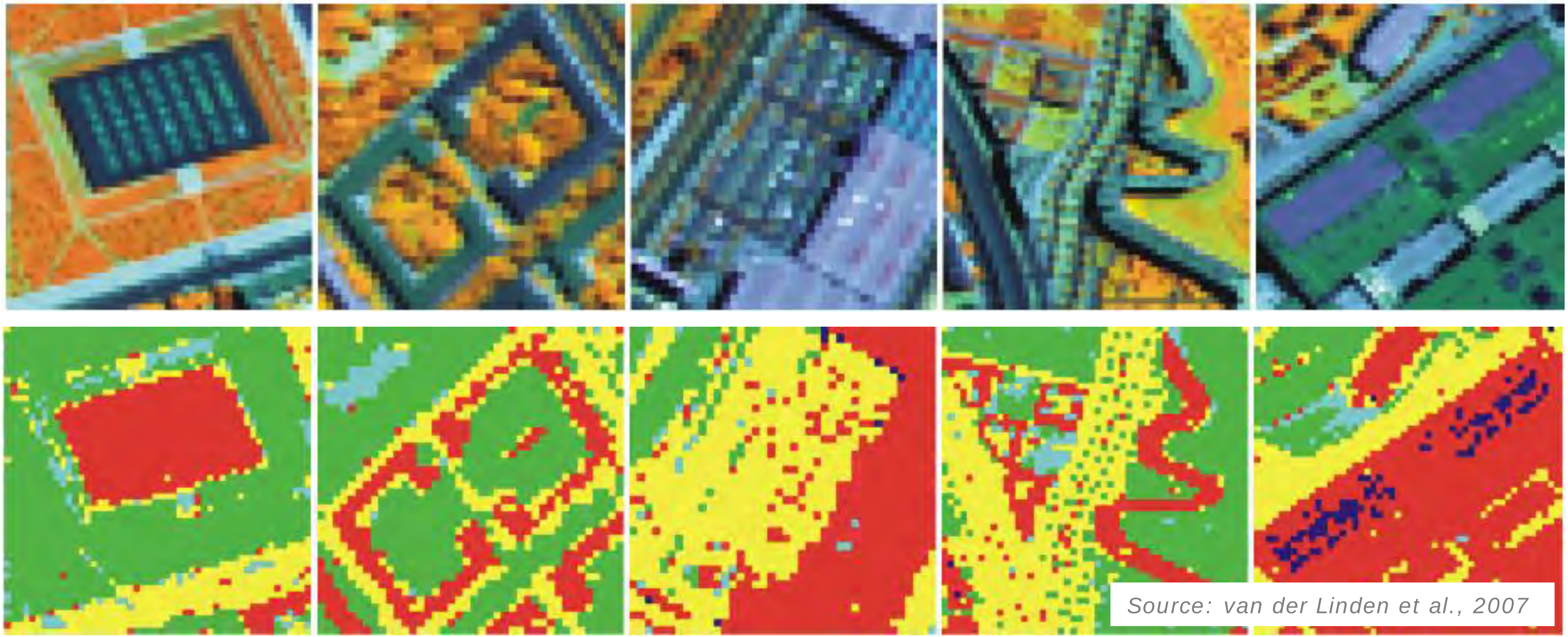

Source: van der Linden et al., 2007

Mapping urban composition using spectral and lidar data

Land cover maps from APEX (2 m; 252 bands) and LiDAR data.

SVC classification with post-processing.

Height/shadow information to account for spectral ambiguity.

High share of pure pixels and high Accuracies.

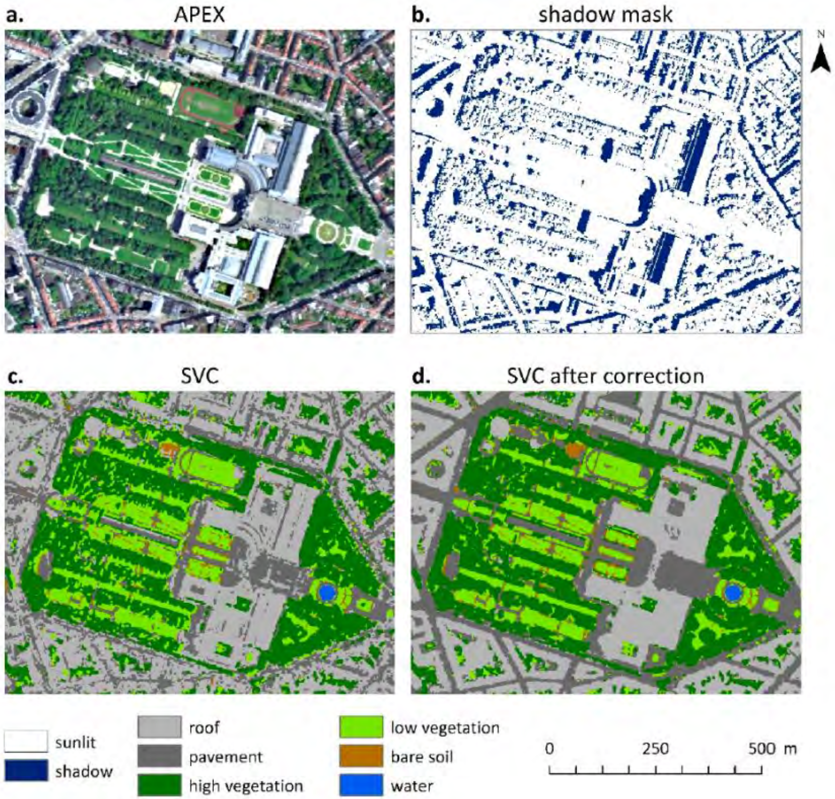

Source: Priem & Canters, 2016

Land Cover	SVC	Cor. (Height)	Cor. (Slope)	Cor. (Roughness)	Cor. (All)
1. red ceramic tile	0.82	0.82	**0.88**	0.82	**0.88**
2. dark ceramic tile	0.81	0.95	**0.95**	0.81	**0.99**
3. dark shingle	0.51	0.51	**0.94**	0.50	**0.94**
4. bitumen	0.77	0.79	**0.90**	0.76	**0.93**
5. fiber cement	0.85	0.84	0.79	0.85	*0.75*
6. bright roof material	0.55	**0.64**	0.55	0.55	**0.63**
7. reflective hydrocarbon	0.75	**0.90**	0.81	0.73	**0.95**
8. gray metal	0.82	0.83	0.78	0.82	0.76
9. green metal	0.95	0.97	0.97	0.95	0.97
10. paved roof	0.87	0.89	0.87	0.87	0.88
11. glass	0.91	0.89	0.91	0.91	0.89
12. gravel roofing	0.71	**0.81**	0.69	0.70	**0.83**
13. extensive green roof	0.84	**1.00**	0.83	0.84	**1.00**
14. solar panel	1.00	1.00	*0.96*	1.00	*0.95*
15. asphalt	0.90	**0.98**	0.92	0.95	0.92
16. concrete	0.52	**0.71**	**0.62**	0.51	**0.71**
17. red concrete pavers	0.83	**1.00**	0.78	0.79	**1.00**
18. railroad track	0.83	*0.70*	0.80	**0.98**	**0.98**
19. cobblestone	0.59	**0.75**	0.53	0.62	**0.69**
20. bright gravel	0.90	*0.72*	0.90	0.90	*0.72*
21. red gravel	0.96	0.96	**1.00**	0.96	*0.89*
22. tartan	1.00	1.00	1.00	1.00	1.00
23. artificial turf	0.98	0.98	*0.93*	0.98	0.97
24. green surface	1.00	1.00	1.00	1.00	1.00
25. high vegetation	1.00	0.85	1.00	1.00	1.00
26. low vegetation	0.80	**0.94**	0.80	0.80	**0.94**
27. bare soil	0.93	*0.85*	0.92	0.93	*0.85*

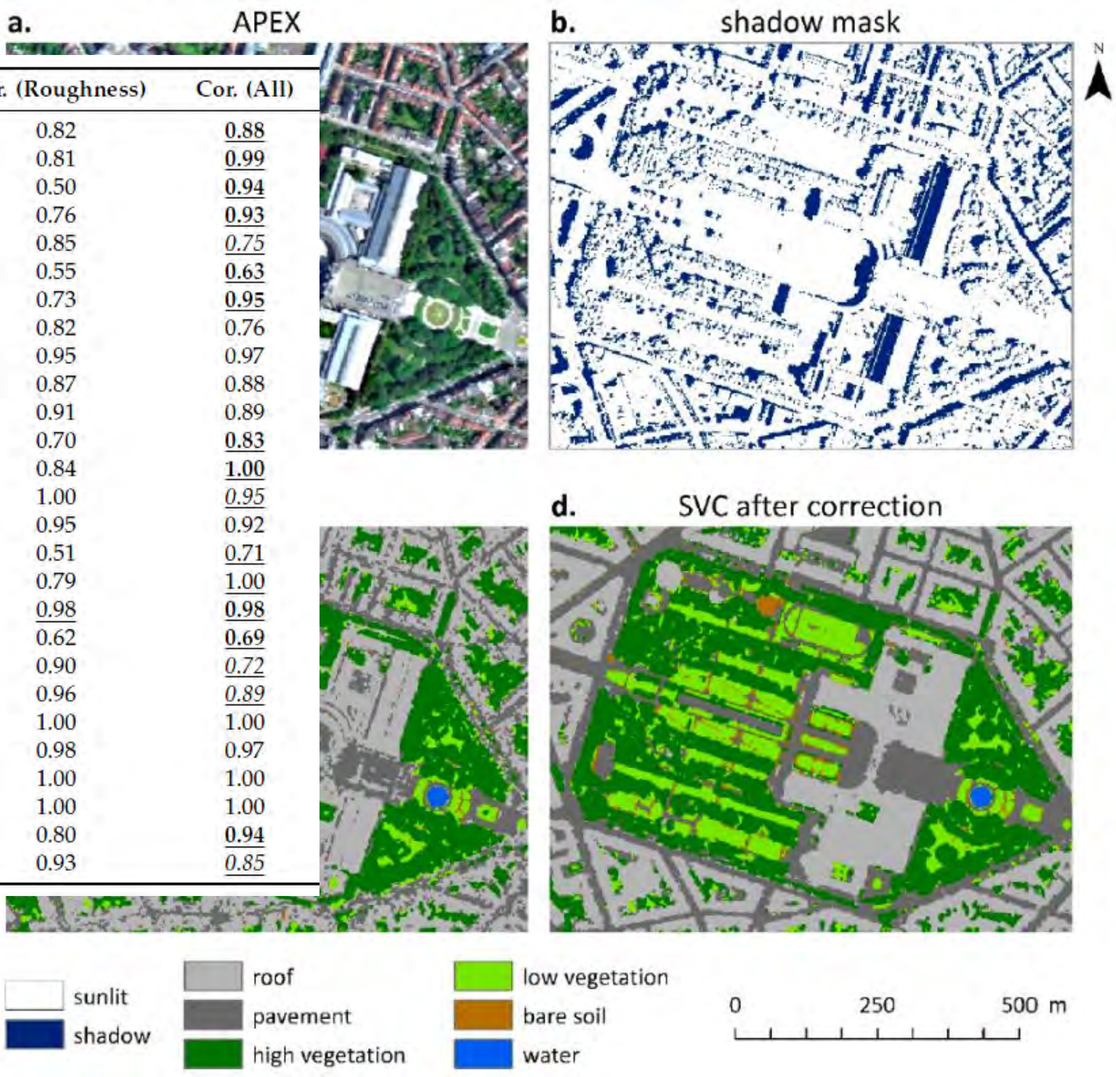

Source: Priem & Canters, 2016

Mapping class fractions from spectral data

Given the high number of mixed pixels in spaceborne data, fraction mapping appears more useful than classification to describe urban composition.

Concepts for quantitative mapping most often assume a linearly mixed spectrum, which can be decomposed into "pure" components, e.g. by linear spectral mixture analysis.

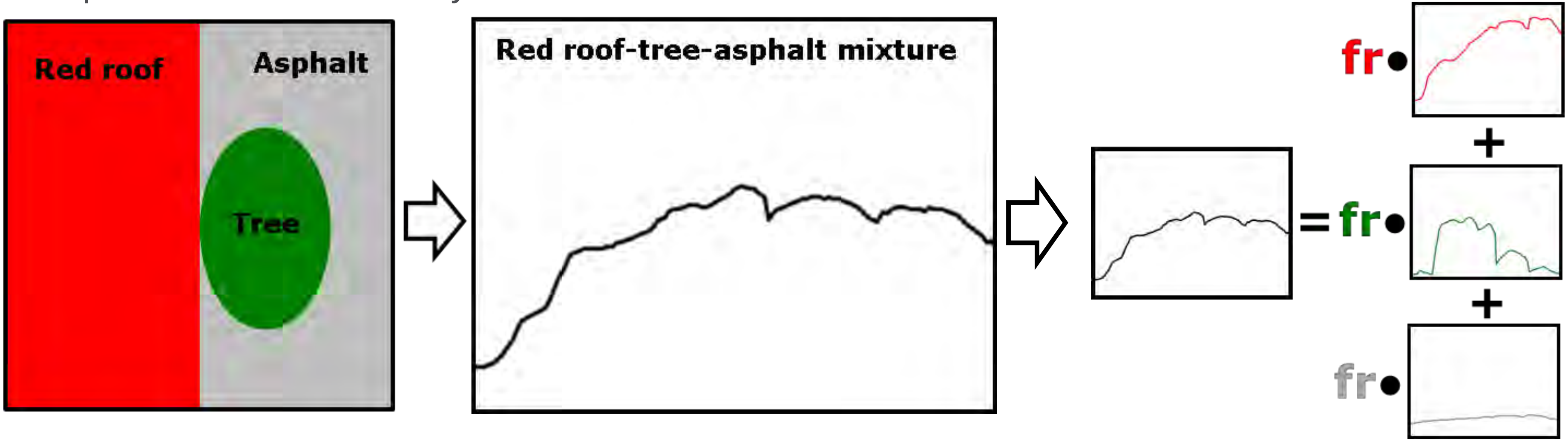

Mapping class fractions from spectral data

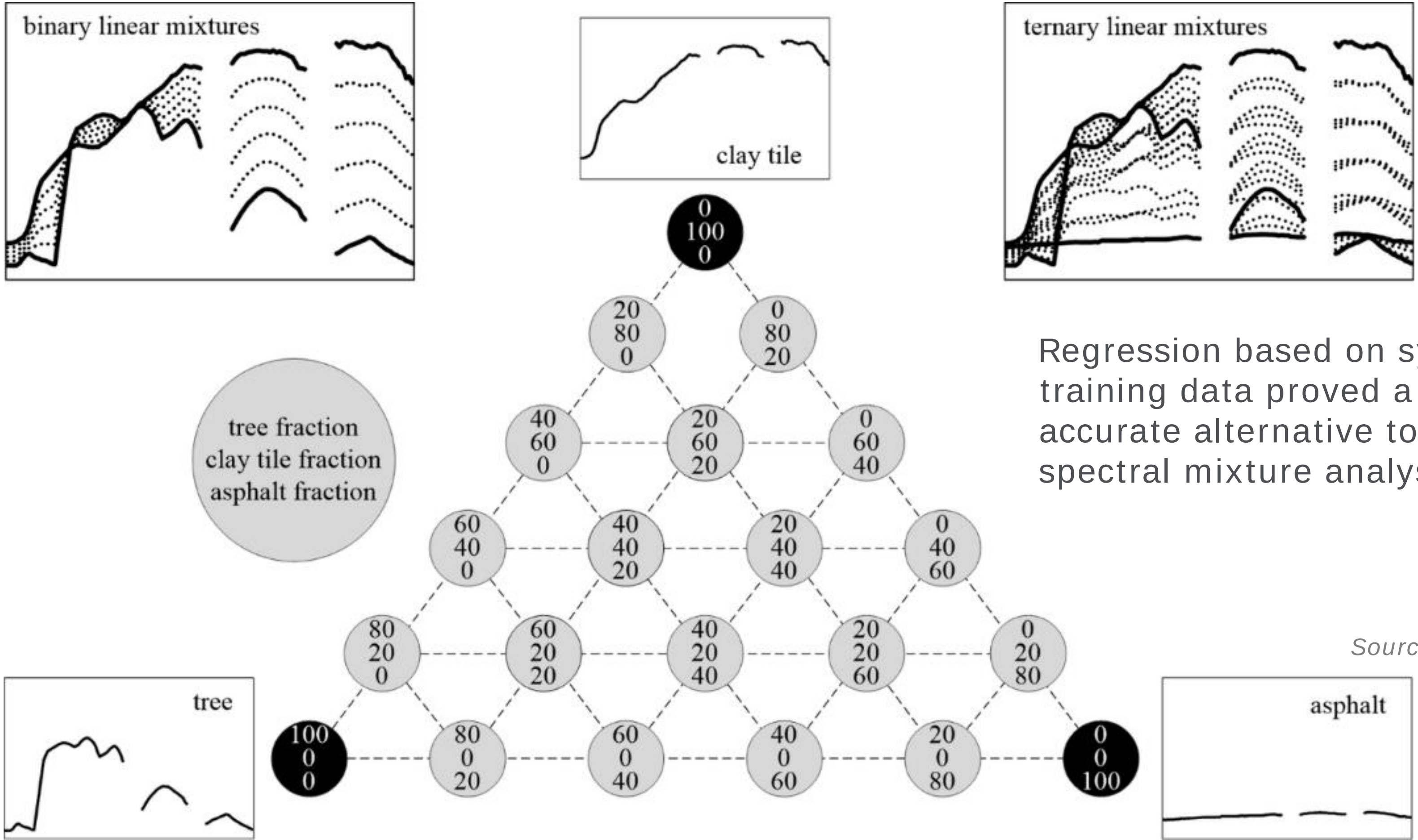

Regression based on synthetic training data proved a reliable and accurate alternative to linear spectral mixture analysis.

Source: Okujeni et al., 2017

Mapping class fractions from spectral data

VIS components can be modelled at high accuracy using SVR with synthetic mixtures.

The decrease in accuracy from 9 m to 30 m is relatively low.

Hyperspectral EnMAP data leads to slightly better results than Landsat data.

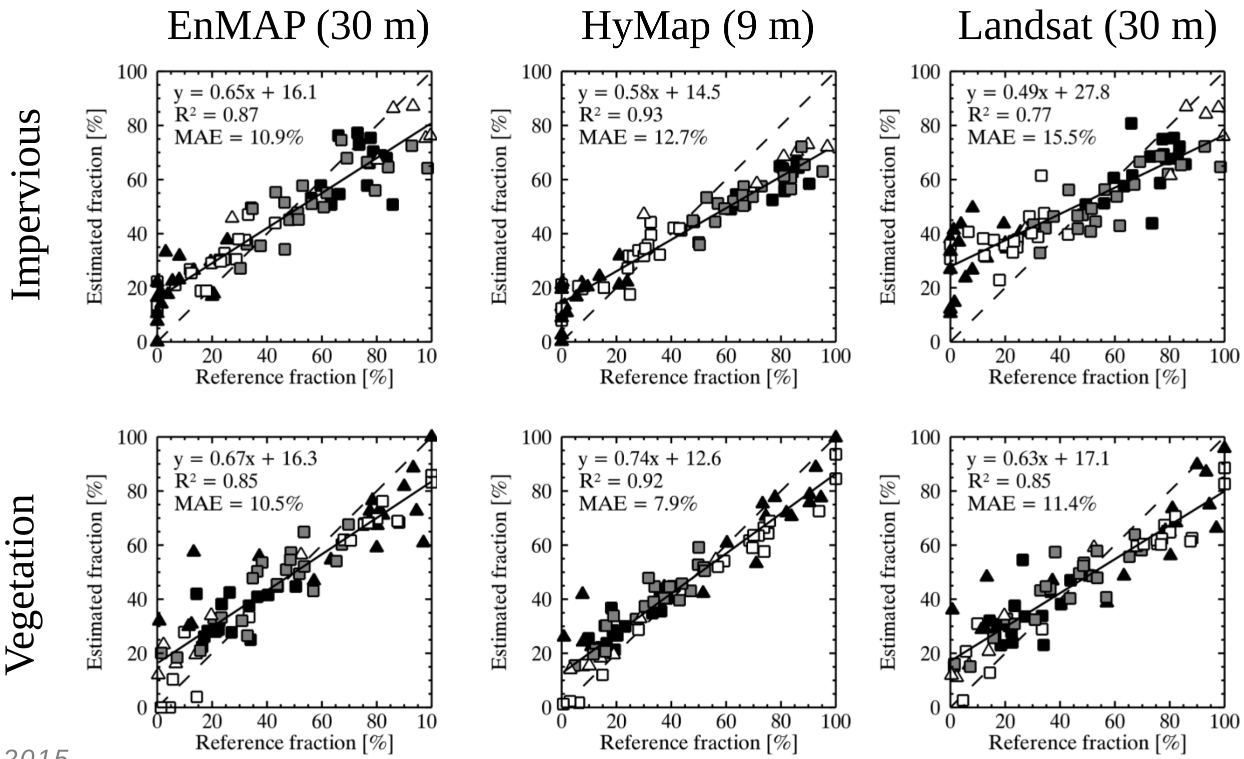

Source: Okujeni et al., 2015

Mapping class fractions from spectral data

The importance for sub-pixel analysis and mapping of fractions is illustrated by an analysis of frequency of extended VIS cover in image data at different resolutions.

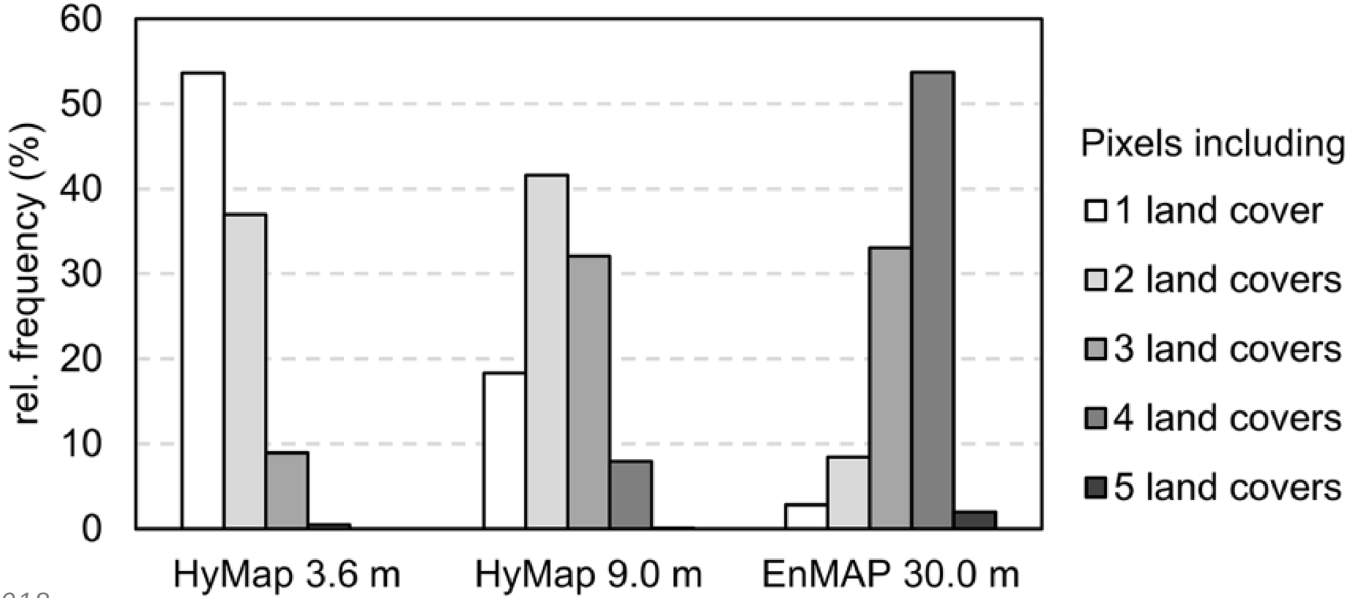

Source: van der Linden et al., 2018

Mapping class fractions from spectral data

Accordingly, the number of mixed pixels increases at coarser resolutions, i.e. pure class colors appear mixed in fraction map.

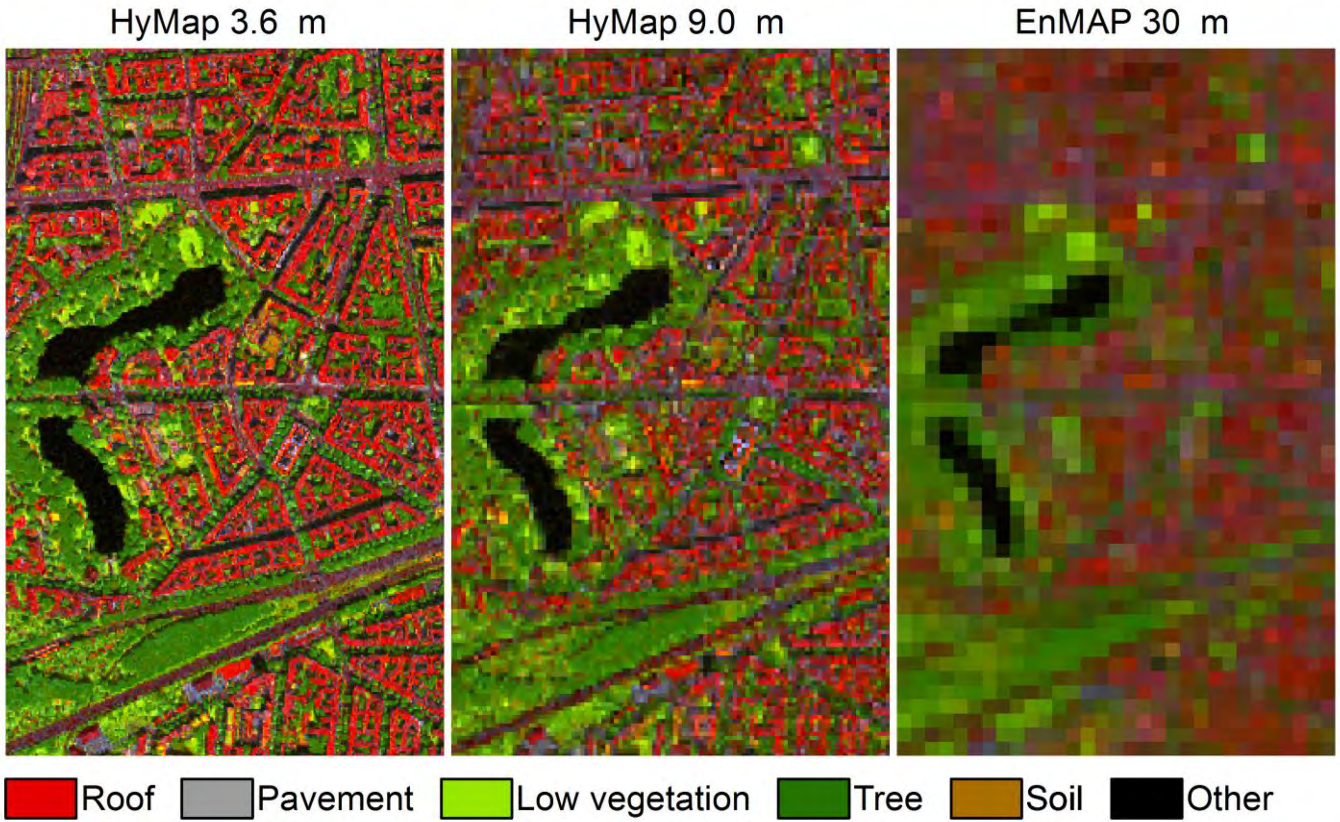

Source: van der Linden et al., 2018

Mapping class fractions from spectral data

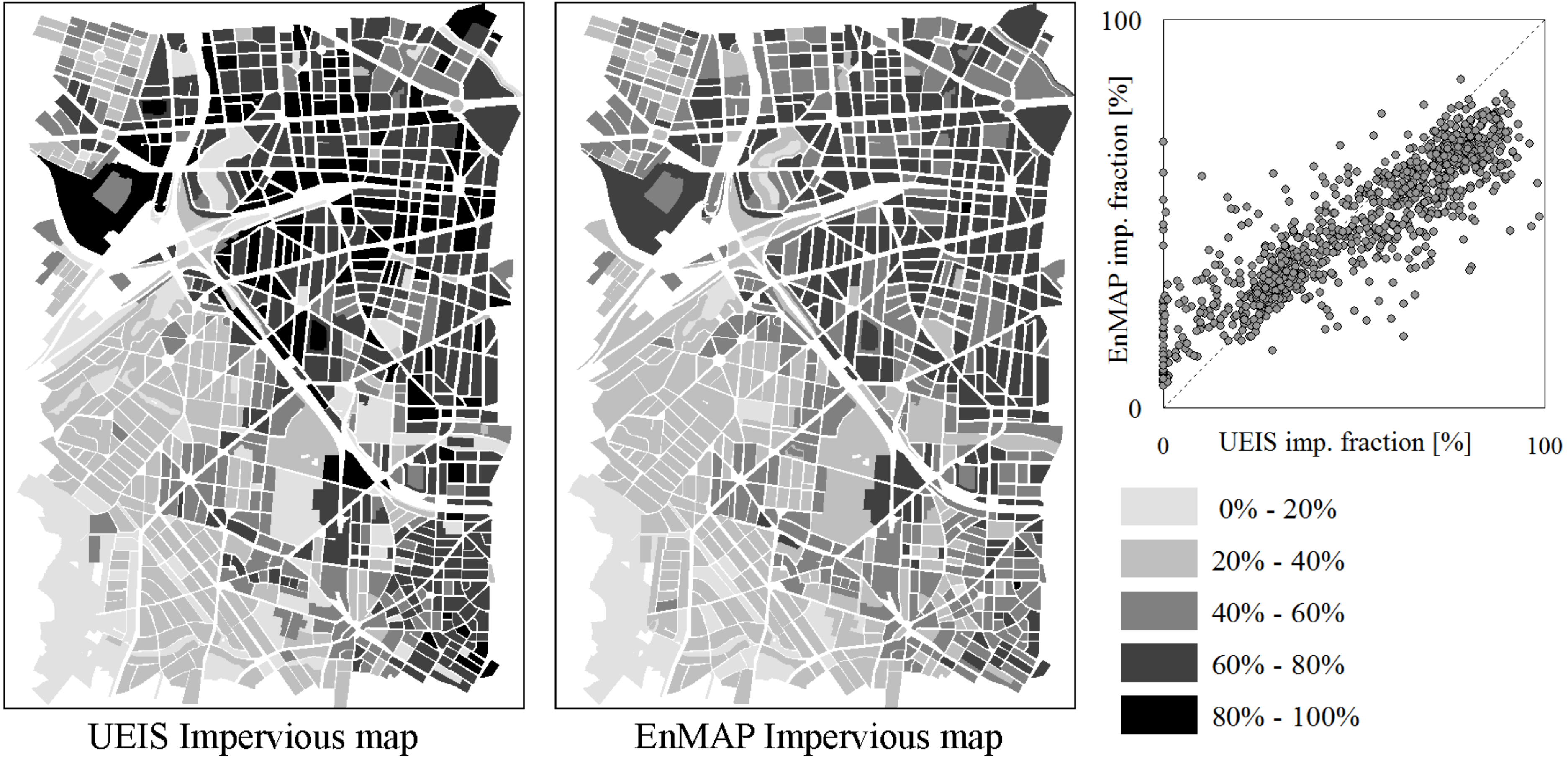

Synthesis

Remote sensing of urban areas at high to very high resolutions is important.

Even at 10-20 resolutions a high number of mixed pixels prevails.

Quantitative maps of (sub-pixel) land cover fractions are needed to describe urban land surfaces with spaceborne remote sensing data.

Approaches for reliable and accurate fraction mapping are needed for urban remote sensing.

→ The practical will introduce you to regression-based mapping of urban areas!

References

Small, Okujeni, van der Linden, Waske (*2018*). In S. Liang: Comprehensive Remote Sensing.

Alonzo *et al.* (2014). Remote Sensing of Environment, 148, 70-83.

Griffiths *et al.* (2010). Remote Sensing of Environment, 114, 426-439.

van der Linden *et al.* (2007). Journal of Applied Remote Sensing, 1.

van der Linden *et al.* (2018). Surveys in Geophysics, DOI: 10.1007/s10712-018-9486-y.

Okujeni, van der Linden *et al.* (2013). Remote Sensing of Environment, 137, 184-197

Okujeni, van der Linden, Hostert (2015). Remote Sensing of Environment 108, 69-80.

Okujeni, van der Linden *et al.* (2017). J. of Selected Topics in Applied Remote Sensing, 10, 1640-1650.

Priem, Canters (2016). Remote Sensing, 8, 787

Ridd (1995). Int. Journal of Remote Sensing, 16, 2165-2185.

Small (2005). Int. Journal Remote Sens., 26, 661-681.

Small, Elvidge (2012). Int. Journal of Applied Earth Observation and Geoinformation. 22, 40-52.

Taubenböck *et al.* (2012). Remote Sensing of Environment, 117, 162-176.

United Nations (2014). World polulation prospects. https://esa.un.org/unpd/wpp/

Schug *et al.* (2018). Remote Sensing of Environment, 210, 217-228

If not indicated differently, figures are taken from the dissertations of S. van der Linden and A. Okujeni. See edoc.hu-berlin.de.

Thank you for your attention!

Geomatics Lab @ HU Berlin

Supported by:

Federal Ministry
for Economic Affairs
and Energy

on the basis of a decision
by the German Bundestag

EnMAP
Hyperspectral Imager

UrbanEARS

Belgian Science Policy Office
belspo

@HumboldtRemSens